

Mice with *Shank3* Mutations Associated with ASD and Schizophrenia Display Both Shared and Distinct Defects

Highlights

- Major psychiatric disorders share many risk genes
- Two mouse lines with ASD-linked and schizophrenia-linked mutations were studied
- Two mutant lines show both shared and distinct synaptic and behavioral phenotypes
- Both developmental and molecular differences were detected in the two mutant lines

Authors

Yang Zhou, Tobias Kaiser,
Patrícia Monteiro, ..., Feng Zhang,
Zhanyan Fu, Guoping Feng

Correspondence

fengg@mit.edu

In Brief

Zhou et al. demonstrate that different alleles of the *Shank3* gene found in ASD and schizophrenia patients have both shared and distinct phenotypes at molecular, synaptic, and circuit levels in mice, which may inform exploration of these relationships in human disorders.

Mice with *Shank3* Mutations Associated with ASD and Schizophrenia Display Both Shared and Distinct Defects

Yang Zhou,^{1,6} Tobias Kaiser,¹ Patrícia Monteiro,^{1,4,5} Xiangyu Zhang,¹ Marie. S. Van der Goes,¹ Dongqing Wang,¹ Boaz Barak,¹ Menglong Zeng,^{1,7} Chenchen Li,^{1,4} Congyi Lu,^{1,4} Michael Wells,^{1,8} Aldo Amaya,⁴ Shannon Nguyen,⁴ Michael Lewis,⁴ Neville Sanjana,^{1,4} Yongdi Zhou,⁶ Mingjie Zhang,⁷ Feng Zhang,^{1,2,3,4} Zhanyan Fu,^{1,4} and Guoping Feng,^{1,2,4,*}

¹McGovern Institute for Brain Research

²Department of Brain and Cognitive Sciences

³Department of Biological Engineering

Massachusetts Institute of Technology, Cambridge, MA 02139, USA

⁴Stanley Center for Psychiatric Research, Broad Institute of MIT and Harvard, Cambridge, MA 02142, USA

⁵PhD Program in Experimental Biology and Biomedicine (PDBEB), Center for Neuroscience and Cell Biology, University of Coimbra, 3000-214 Coimbra, Portugal

⁶Key Laboratory of Brain Functional Genomics, Ministry of Education, Shanghai Key Laboratory of Brain Functional Genomics, Institute of Cognitive Neuroscience, School of Psychology and Cognitive Science, East China Normal University, Shanghai 200062, China

⁷Division of Life Science, Center of Systems Biology and Human Health, State Key Laboratory of Molecular Neuroscience, Hong Kong University of Science and Technology, Hong Kong

⁸Department of Neurobiology, Duke University Medical Center, Durham, NC 27710, USA

*Correspondence: fengg@mit.edu

<http://dx.doi.org/10.1016/j.neuron.2015.11.023>

SUMMARY

Genetic studies have revealed significant overlaps of risk genes among psychiatric disorders. However, it is not clear how different mutations of the same gene contribute to different disorders. We characterized two lines of mutant mice with *Shank3* mutations linked to ASD and schizophrenia. We found both shared and distinct synaptic and behavioral phenotypes. Mice with the ASD-linked InsG3680 mutation manifest striatal synaptic transmission defects before weaning age and impaired juvenile social interaction, coinciding with the early onset of ASD symptoms. On the other hand, adult mice carrying the schizophrenia-linked R1117X mutation show profound synaptic defects in prefrontal cortex and social dominance behavior. Furthermore, we found differential *Shank3* mRNA stability and SHANK1/2 upregulation in these two lines. These data demonstrate that different alleles of the same gene may have distinct phenotypes at molecular, synaptic, and circuit levels in mice, which may inform exploration of these relationships in human patients.

INTRODUCTION

Although schizophrenia and autism are two different disorders (DSM-5), it has long been proposed that they share some common pathologies and symptoms (de Lacy and King, 2013).

Currently, the etiologies of schizophrenia and autism are largely unknown, but recent human studies highlight the contribution of genetic risk factors to both disorders (Schizophrenia Working Group of the Psychiatric Genomics Consortium, 2014; De Rubeis et al., 2014). In particular, mutations in a group of genes linked to synaptic development, function, and plasticity were frequently identified in patients diagnosed with either schizophrenia or autism (Kenny et al., 2014), suggesting that genetic mutations leading to dysregulation of synaptic transmission play critical roles in the pathophysiology of both disorders (De Rubeis et al., 2014; Fromer et al., 2014). Interestingly, recent genetic studies further revealed significant overlaps of risk genes across major psychiatric disorders including schizophrenia, bipolar disorder, major depressive disorder, and autism (Lee et al., 2013; Cross-Disorder Group of the Psychiatric Genomics Consortium, 2013). Furthermore, large-scale exome sequencing of autism spectrum disorder (ASD) and schizophrenia patient DNA samples has identified many of the same genes in both disorders, suggesting that different mutations in the same gene can cause/contribute to different disorders (Guilmatre et al., 2014; McCarthy et al., 2014).

One such example is the *SHANK3* gene (Boeckers et al., 1999; Naisbitt et al., 1999). SHANK family members share five main domain regions: N-terminal ankyrin repeats, SH3 domain, PDZ domain, proline-rich region, and a C-terminal SAM domain. Through these functional domains, SHANK interacts with many postsynaptic density (PSD) proteins. Most notably, SHANK binds to SAPAP, which in turn binds to PSD95 to form the PSD95/SAPAP/SHANK postsynaptic complex (Kim and Sheng, 2004). Together, these three groups of multi-domain proteins are proposed to form a key scaffold, orchestrating the assembly of the macromolecular postsynaptic signaling complex at

glutamatergic synapses. This complex has been shown to play an important role in targeting, anchoring, and dynamically regulating synaptic localization of neurotransmitter receptors and signaling molecules (McAllister, 2007). SHANK is also connected to the mGluR pathway through its binding to Homer (Tu et al., 1999). In addition, given its link to actin-binding proteins, SHANK has been shown to regulate spine development (Roussignol et al., 2005; Sala et al., 2001).

Deletion of *SHANK3* has been shown to be the cause of core neurodevelopmental and neurobehavioral deficits in Phelan-McDermid syndrome (PMS), an autism spectrum disorder with symptoms that include intellectual disability, autistic behaviors, hypotonia, and impaired development of speech and language (Wilson et al., 2003). Subsequent genetic screens also identified a variety of mutations in the *SHANK3* gene in ASD patients not diagnosed with PMS including a guanine nucleotide insertion in exon 21 of *SHANK3* gene (position 3680) from two brothers diagnosed with ASD accompanied by severe mental retardation (Durand et al., 2007; Gauthier et al., 2009; Moessner et al., 2007). These data implicate *SHANK3* gene disruption/mutation as a monogenic cause of ASD. In support of these genetic findings, studies of *Shank3* mutant mice from our laboratory and others have revealed various degrees of synaptic dysfunction and autistic-like behaviors (Bozdagi et al., 2010; Kouser et al., 2013; Peça et al., 2011; Wang et al., 2011b). In addition, duplication of the *SHANK3* gene was found in patients diagnosed with bipolar disorders and mice with *Shank3* overexpression exhibit synaptic dysfunction and manic-like phenotypes (Han et al., 2013).

Interestingly, a non-sense mutation of *SHANK3* changing an arginine to stop codon (R1117X) was identified from three brothers diagnosed with schizophrenia/schizoaffective disorder between ages 16 and 21 without showing obvious autistic features during their childhood (Gauthier et al., 2010). The three brothers also had mild-to-moderate mental retardation, which is often seen, and generally more severe, in ASD patients with *SHANK3* mutations. Understanding the mechanisms by which different mutations in the same gene lead to different disorders will likely shed light on both shared and unique neural mechanisms of these disorders. We therefore created two mutant mouse lines. The first line harbors the ASD patient-linked single guanine nucleotide (G) insertion at cDNA position 3680 and leads to a frameshift and downstream stop codon (*InsG3680* mutation). The second line contains the schizophrenia patient-linked point mutation and changes arginine 1117 to a stop codon (R1117X mutation). We performed systematic comparisons between the two mutant lines at molecular, cellular, synaptic, and behavioral levels and found both distinct and shared defects in these two mutant models. In particular, we found that mutant mice with the ASD-linked *InsG3680* mutation, but not with the schizophrenia-linked R1117X mutation, manifest defective synaptic transmission in the striatum before weaning age, as well as impaired juvenile social play behavior, coinciding with the early onset of ASD symptoms in human patients. On the other hand, adult mice with the R1117X mutation, but not with the *InsG3680* mutation, show synaptic defects in prefrontal cortex, consistent with clinical findings implicating prefrontal cortex defects in schizophrenia patients. Biochemical studies revealed

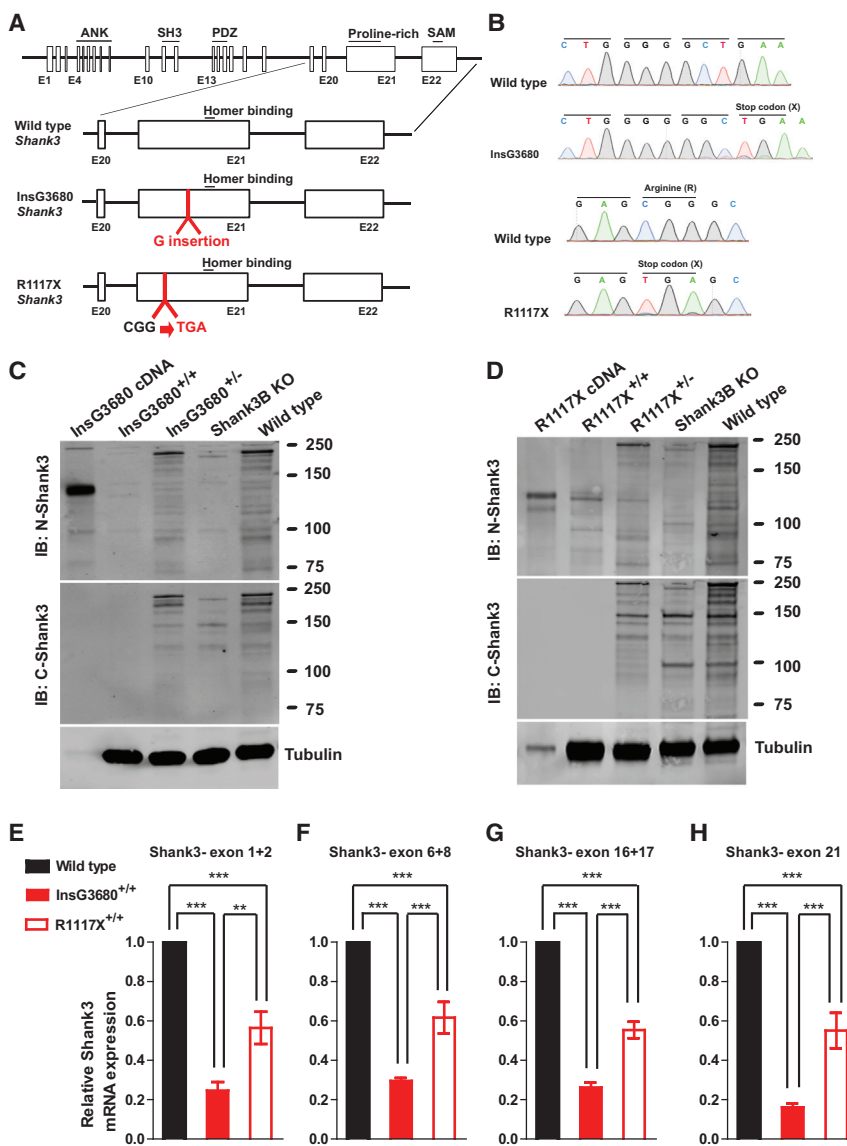
both common and differential defects in postsynaptic signaling complexes and differential compensatory mechanisms in these two mutant lines. Behaviorally, both lines of mutant mice exhibit anxiety-like behavior and social interaction deficits. However, *InsG3680* mutant mice show stronger repetitive/compulsive grooming behavior, whereas R1117X mutant mice show stronger allogrooming and social dominance-like behavior. Together, our study potentially provides a mechanistic explanation on how distinct mutations of the *Shank3* gene may lead to distinct molecular, synaptic, and circuit defects and relevant behavior abnormalities.

RESULTS

Distinct Effects of *InsG3680* and R1117X Mutations on *SHANK3* Protein and mRNA

Shank3 is a very complex gene at the transcript level because of multiple intragenic promotors and alternative splicing (Wang et al., 2011b; Wang et al., 2014b). Both *InsG3680* and R1117X mutations are in exon 21, which is common to most if not all isoforms, and the two mutations were separated by only 325 nucleotides (Figure 1A). For *InsG3680* mutation, we placed the G insertion at position 3680 in *Shank3*, which causes a frameshift and a stop codon immediately after the G insertion (Figures 1A and 1B). For the R1117X mutation, we changed arginine (R) codon "CGG" to stop codon "TGA" to introduce the "R" to "X" mutation at amino acid position 1117 as described in the finding from schizophrenia patients (Figures 1A and 1B). We generated a C57 B6/S129 Sv mixed background mice population for all experiments performed in this study unless otherwise specified. Both homozygous *InsG3680* and R1117X *Shank3* mutant mice are viable and fertile.

The predicted sizes of the resulting truncated proteins are 135 kDa for *InsG3680* mutation and 122 kDa for R1117X mutation, respectively. To examine whether such truncated SHANK3 proteins exist in the brain, we prepared postsynaptic density (PSD) fractions from striatal tissue and probed with antibodies recognizing epitopes located at either the N terminus (located upstream of both mutations) or C terminus of the SHANK3 protein (located downstream of both mutations; Table S1). When probed with the C terminus antibody, no signals above 75 kDa were detected in striatal PSD preparations from either homozygous *InsG3680* mutant mice (*InsG3680*^{-/-}) or R1117X mutant mice (R1117X^{-/-}) (Figures 1C and 1D), consistent with the fact that the C terminus antibody recognizes epitopes that are beyond the premature stop codons caused by the *InsG3680* and R1117X mutations. In contrast, when probed with an antibody raised against the N terminus of SHANK3 (Neuromab 367/62), we detected truncated SHANK3 bands in striatal PSD preparations from the R1117X mutant mice with the major band matching the predicted 122 kDa expressed in HEK293 cells (Figure 1D). However, no clear signals were detected in striatal PSD preparations from *InsG3680* mutant mice (Figure 1C). Similar results were obtained in PSD preparations from the cortex of R1117X and *InsG3680* mutant mice using N terminus and C terminus antibodies. Together, our results reveal that R1117X and *InsG3680* mutations have distinct effects on SHANK3 protein expression.



Since non-sense mutations could lead to reduced mRNA levels through non-sense-mediated decay (NMD) of abnormal mRNAs (Frischmeyer and Dietz, 1999), we examined *Shank3* mRNA levels in the striatum of InsG3680 and R1117X mutant mice by quantitative real-time PCR. Due to the extensive alternative splicing of multiple coding exons in the *Shank3* gene (Wang et al., 2011b), we designed four pairs of primers probing different coding regions to minimize the potential detection bias caused by alternative splicing. We consistently observed dramatically reduced levels of *Shank3* mRNA from striatal tissue of InsG3680^{+/-} mice with all four pairs of probes (Figures 1E–1H). Interestingly, striatal tissues from R1117X^{+/-} mice showed significantly higher levels of *Shank3* mRNA than from InsG3680^{+/-} mice (Figures 1E–1H). These results suggest that *Shank3* mRNAs with the R1117X mutation are more stable than mRNAs with the InsG3680 mutation, consistent with our result that trun-

Figure 1. Genetically Engineered Mice with InsG3680 or R1117X *Shank3* Mutation Differentially Express SHANK3 Protein and mRNA

(A) Schematic diagram for wild-type *Shank3*, InsG3680-, and R1117X-targeted *Shank3* alleles. Gene structure of wild-type mouse *Shank3* gene and magnified panels on the structure between exon 20 and exon 22 are shown below. Top: wild-type *Shank3*; middle: autism-associated InsG3680 *Shank3* mutation with an insertion of “guanine” nucleotide at position 3680; bottom: schizophrenia-associated R1117X *Shank3* mutation changing the “CGG” codon for arginine to a “TGA” stop codon.

(B) Representative sequencing chromatograms of wild-type and InsG3680 mutated alleles; wild-type and R1117X mutated alleles showing the point mutations.

(C) Representative western blots using striatal PSD fractions prepared from wild-type, *Shank3B* KO mice, InsG3680^{+/-} mice, InsG3680^{+/+} mice; lysate from HEK239 cells expressing cDNA plasmid encoding the InsG3680 mutated *Shank3*. Note that neither the antibody against the N nor C terminus detected SHANK3 protein in InsG3680^{+/-} mice.

(D) Representative western blots using striatal PSD fractions prepared from wild-type, *Shank3B* KO mice, R1117X^{+/-} mice, R1117X^{+/+} mice; lysate from HEK239 cells expressing cDNA plasmid encoding the R1117X mutated *Shank3*. Note that SHANK3 protein expression is almost abolished except for a prominent truncated isoform in the R1117X^{+/-} line that is detected with the antibody against the N terminus.

(E–H) The relative level of *Shank3* mRNA in striatum is different between the two lines as quantified by primers amplifying exon 1 to 2, exon 6 to 8, 16 to 17, and partial exon 21 before both *Shank3* mutation sites. Data are normalized to *Gapdh* mRNA and presented as mean ± SEM. **p < 0.01, ***p < 0.001; one-way ANOVA with Bonferroni post hoc test, WT mice (n = 5), R1117X^{+/+} mice (n = 5) and InsG3680^{+/-} mice (n = 5).

cated SHANK3 proteins are present in R1117X^{+/-} mice. Together, our data suggest that the ASD-linked InsG3680 mutation results in an almost complete loss of SHANK3 protein, which is consistent with the full deletion of the *SHANK3* gene identified in most Phelan-McDermid Syndrome patients (Bonaglia et al., 2011; Wilson et al., 2003). In contrast, the schizophrenia-linked R1117X mutation results in the generation of truncated SHANK3 protein, which could potentially either be partially functional or act in a dominant-negative form.

InsG3680 Mutants Exhibit Early Striatal Synaptic Transmission Defects and Impaired Social Interaction

Since ASD patients with *SHANK3* mutations are usually diagnosed before the age of 3, whereas the schizophrenia patients carrying the R1117X mutation were diagnosed between ages 16 and 21, we wondered whether these two mutated mice

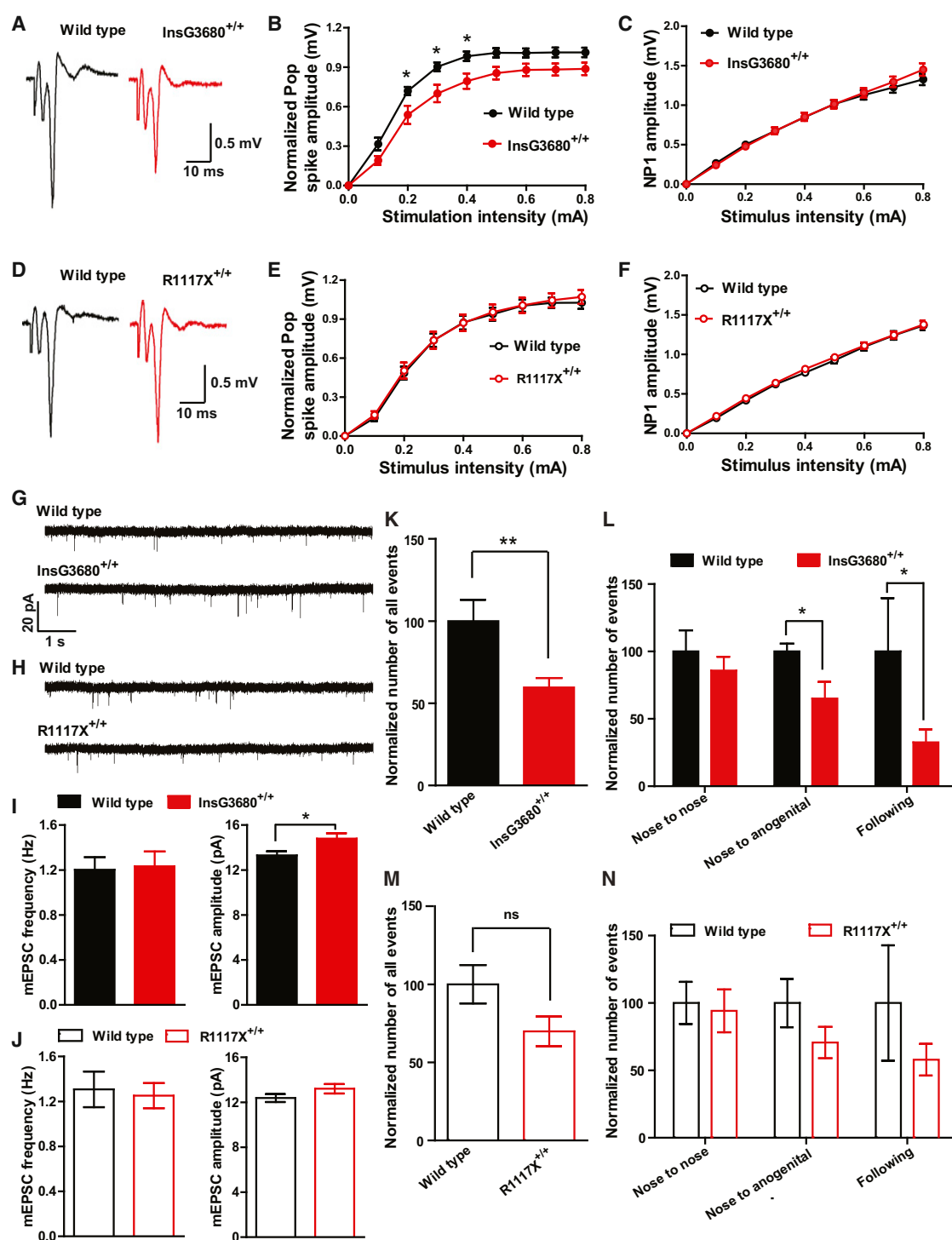


Figure 2. InsG3680^{+/+} but Not R1117X^{+/+} Mice Display Altered Striatal Synaptic Transmission at P14 and Reduced Social Interaction at P23
 (A and D) Representative cortico-striatal pop spike traces recorded from P14 mice with indicated genotypes.
 (B and C) Cortical-striatal input-output curve shows reduced pop spike responses in InsG3680^{+/+} mice compared to wild-type littermates. NP1 amplitude is similar between the genotypes, suggesting that presynaptic input is not different.
 (E and F) Cortical-striatal input-output curve shows similar pop spike responses and NP1 amplitude between R1117X^{+/+} mice and their wild-type littermates.
 In (B), (C), (E), and (F), data are presented as mean \pm SEM. *p < 0.05; two-way ANOVA repeated-measures with Bonferroni post hoc test. n = 12 slices from 4 pairs of littermates for each cohort.

(legend continued on next page)

exhibit any differential defects at early developmental stages. Since *Shank3* is the only Shank family gene highly expressed in the striatum, we first examined the strength of evoked population spike responses in the striatum by performing field recordings in dorsolateral striatum at postnatal day 14 (P14). We found that *InsG3680*^{+/+} mice have reduced field population spikes at postnatal day 14 (**Figures 2A** and **2B**). In contrast, no difference was found between *R1117X*^{+/+} mice and their wild-type littermate controls (**Figures 2D** and **2E**). Presynaptic function seems unaffected, as indicated by the relationship of stimulation intensity to amplitude of negative peak 1 (**Figures 2C** and **2F**). We further measured other synaptic parameters including evoked AMPA to NMDA current ratio and miniature EPSCs by whole-cell patch-clamping recordings of dorsolateral striatal medium spiny neurons (MSNs). Through pharmacologically isolating evoked AMPA and NMDA current as described previously ([Saal et al., 2003](#)), we detected no change of AMPA to NMDA current ratio in both mutants as compared to their wild-type (**Figure S1**). No change of miniature EPSC (mEPSC) frequency was detected from both mutants as compared to wild-type controls (**Figures 2G–2J**). Interestingly, we observed significant increase of mEPSC amplitude in *InsG3680*^{+/+} mutants (**Figures 2G** and **2I**), which may suggest a compensatory mechanism of MSNs in the presence of evoked synaptic transmission defects.

We next examined how the two mutations may affect the expression of synaptic proteins in the striatum at P14. We found significantly reduced Homer protein in both *R1117X*^{+/+} and *InsG3680*^{+/+} mice (**Figure S2**). Interestingly, we found that in the striatum of P14 *InsG3680*^{+/+} mice, GluR1 is significantly up-regulated, consistent with the increased AMPA-mediated mEPSC amplitude observed. Several other synaptic proteins including SynGAP, Shank2, and NMDA receptor subunits also show a trend of upregulation (**Figure S2**). Together, our biochemistry data and electrophysiological measurements from evoked and basal synaptic transmission suggest a complex scenario in young *InsG3680*^{+/+} mice in which striatal-evoked population spike responses are reduced but basal AMPA receptor-mediated mEPSC amplitude and GluR1 are increased. This may suggest that at this developmental stage, MSNs are trying to compensate for the defective evoked synaptic transmission by upregulating AMPR receptors in remaining functional synapses.

Although no basic synaptic transmission defects were detected in the striatum of P14 *R1117X*^{+/+} mice, we found that PSD93, SynGAP, and NMDA receptor subunits are reduced in a striatal synaptosomal plasma membrane (SPM) preparation from these mice (**Figure S2**). Furthermore, unlike in the P14 *InsG3680*^{+/+} mice, we did not see a trend of upregulation of any of the synaptic proteins tested. Together, these data suggest that the truncated *R1117X* *Shank3* protein might be partially

functional and its presence is sufficient to maintain basic normal synaptic transmission. To test this hypothesis, we evaluated the ability of the *R1117X* *Shank3* mutant to rescue previously characterized cortico-striatal synaptic dysfunction in our *Shank3B* knockout mice ([Peça et al., 2011](#)) by using a cortico-striatal co-culture system. GFP plasmid alone or GFP plasmid together with *R1117X* *Shank3* mutant plasmid were introduced into primary MSNs derived from *Shank3B* knockout mice through Nucleofection before plating. Transfected MSNs were then co-plated with cortical neurons. Whole-cell patch-clamp recordings of transfected neurons showed that expression of *R1117X* mutants significantly increased the frequency of mEPSCs in *Shank3* knockout MSNs when compared to GFP control neurons (**Figure S3**). These *in vitro* data support the hypothesis that *R1117X* *Shank3* mutant is partially functional in developing MSNs.

To evaluate the behavioral consequence caused by *R1117X* and *InsG3680* *Shank3* mutations at an early developmental stage, we first measured the maternal separation-induced ultrasonic vocalization behavior in pups between postnatal days 2 and 12. We found no significant differences in total number, total duration, mean duration, and peak amplitude of calls among genotypes. We next examined juvenile social play behavior at P23. We found significantly reduced numbers of all interactive events between mouse pairs carrying *InsG3680*^{+/+} mutation as compared to their wild-type littermate controls (**Figure 2K**). By categorizing the reciprocal play behavior into nose-to-nose, anogenital sniffing, and following behavior, we found both the nose-to-anogenital sniffing and following behavior are significantly reduced in *InsG3680*^{+/+} mice (**Figure 2L**). We found a similar trend in *R1117X* mice but it did not reach statistical significance (**Figures 2M** and **2N**). Together, these data indicate an early-onset social interaction deficit in *InsG3680*^{+/+} *Shank3* mutant mice.

Reduced Striatal Synaptic Transmission in Both Adult Mutant Lines

Although *Shank3* is expressed in many brain regions, it is the only Shank family member enriched in the striatum. Our previous studies of young adult homozygous *Shank3B* knockout mice revealed significant synaptic defects in MSNs of the striatum including reduced pop spike responses by field recordings and reduced frequency and amplitude of miniature excitatory postsynaptic current (mEPSC) by whole-cell recordings ([Peça et al., 2011](#)). Here we compared the effects of *InsG3680* and *R1117X* mutations on striatal synaptic function using electrophysiological recording on acutely isolated brain slices. We found both *InsG3680* and *R1117X* homozygous but not heterozygous mice showed reduced pop spike responses (**Figures 3A, 3B, 3D, and 3E**). No differences of presynaptic function

(G and H) Typical AMPA receptor-mediated mEPSC traces recorded from P14 MSNs with indicated genotypes.

(I and J) Amplitude but not frequency of mEPSC is increased in *InsG3680*^{+/+} MSNs compared to wild-type. No change of amplitude or frequency of mEPSC in *R1117X*^{+/+} MSNs. In *InsG3680* cohort, n = 29 neurons for wild-type; n = 29 neurons for *InsG3680*^{+/+} from 3 pairs of littermates; in *R1117X* cohort, n = 30 neurons for wild-type, n = 31 neurons for *R1117X*^{+/+} from 3 pairs of littermates. Data are presented as mean ± SEM; two-tailed t test.

(K and M) Total number of interaction events from mice pairs with indicated genotypes as normalized to wild-type control.

(L and N) Normalized number of categorized interaction events from mice pairs with indicated genotypes as normalized to wild-type control.

In (K), (L), (M), and (N), in *R1117X* cohort, n = 9 pairs of mice for wild-type; n = 9 pairs of mice for *R1117X*^{+/+}; in *InsG3680* cohort, n = 8 pairs of mice for wild-type; n = 10 pairs of mice for *InsG3680*^{+/+}. Data are presented as mean ± SEM, *p < 0.05, **p < 0.01; two-tailed t test.

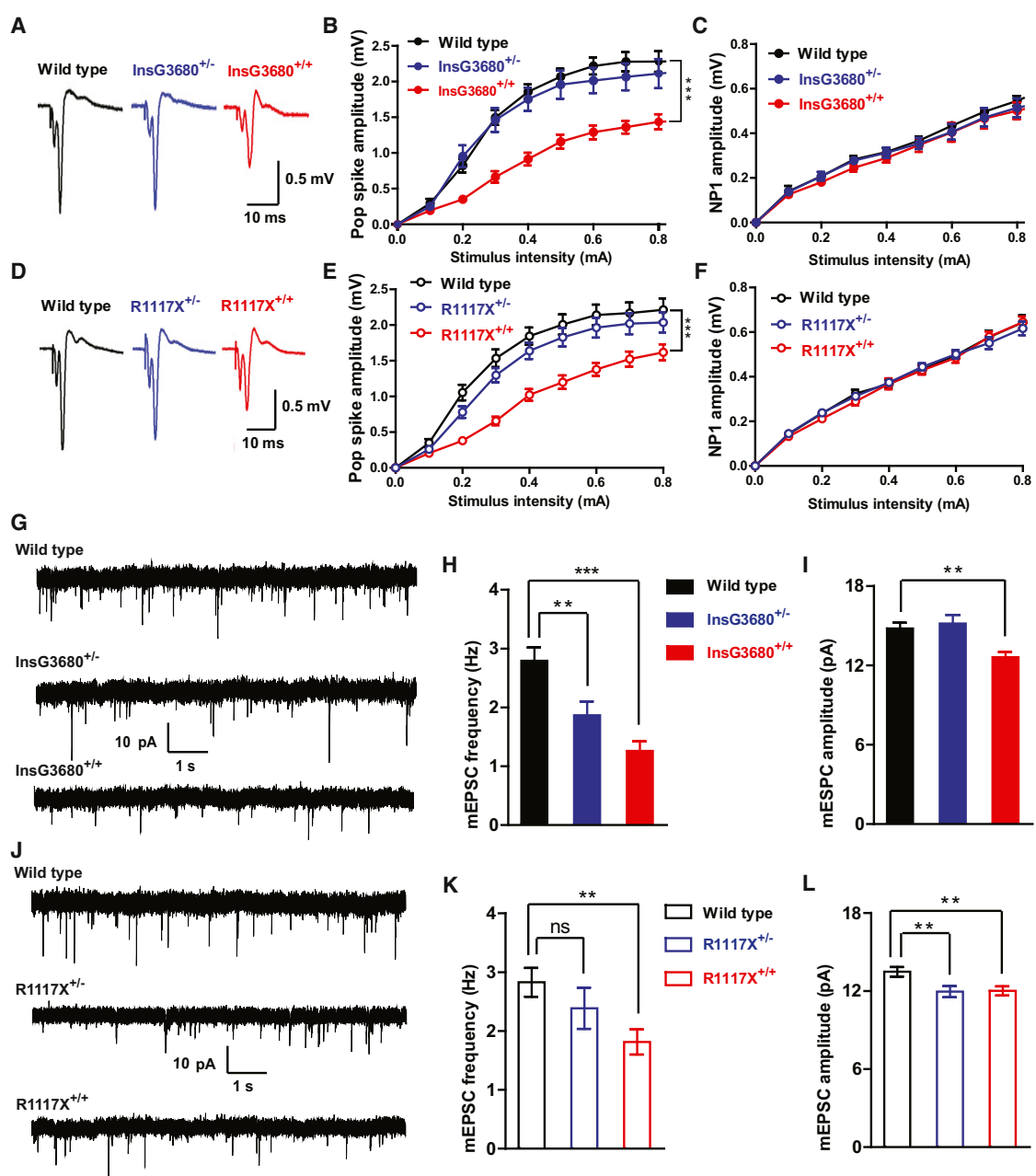


Figure 3. Striatal Synaptic Transmission Is Reduced in Adult R1117X and InsG3680 Mutant Mice

(A and D) Representative cortical-striatal pop spike traces from mice with indicated genotypes.

(B and E) Reduced striatal pop spike amplitude in both $\text{InsG3680}^{+/-}$ and $\text{R1117X}^{+/-}$ mice.

(C and F) No difference of NP1 amplitude among genotypes.

In (B), (C), (E), and (F) data are presented as mean \pm SEM. *** $p < 0.001$; two-way ANOVA repeated-measures with Bonferroni post hoc test. n = 12 slices per genotype from 4 pairs of mice.

(G and J) Typical AMPA receptor-mediated mEPSC traces recorded from MSNs with indicated genotypes.

(H and I) mEPSC frequency of MSNs is reduced in both homozygous and heterozygous InsG3680 mutant mice compared to wild-type littermates. mEPSC amplitude is also reduced in homozygous InsG3680 mutant mice. n = 26 neurons for WT; n = 24 neurons for $\text{InsG3680}^{+/-}$; n = 21 neurons for $\text{InsG3680}^{+/+}$ from three pairs of mice.

(K and L) mEPSC frequency of MSNs is reduced in homozygous R1117X mutant mice compared to wild-type littermates. mEPSC amplitude is reduced in both homozygous and heterozygous R1117X mutant mice. n = 23 neurons for WT; n = 24 neurons for $\text{R1117X}^{+/-}$; n = 26 neurons for $\text{R1117X}^{+/+}$ from three pairs of mice.

In (H), (I), (K), and (L), data are presented as mean \pm SEM. ** $p < 0.01$, *** $p < 0.001$; one-way ANOVA with Bonferroni post hoc test.

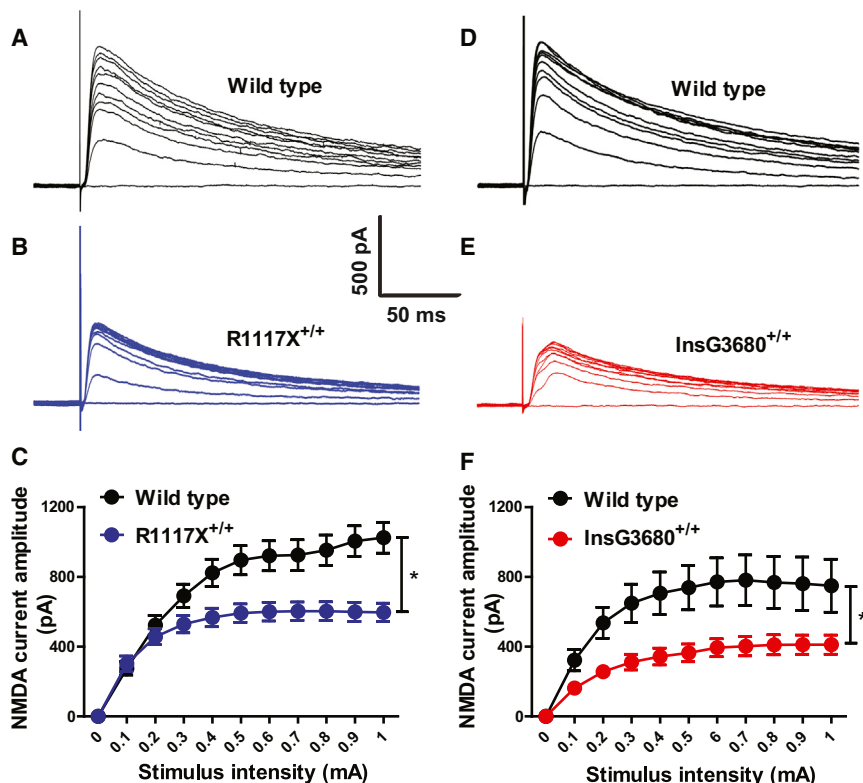


Figure 4. Reduced NMDA Receptors Mediated Synaptic Transmission in Both R1117X^{+/+} and InsG3680^{+/+} Shank3 Mutant Mice

(A–C) Typical NMDA receptors mediated currents from striatal MSNs by stimulating corpus callosum and quantification. n = 16 neurons for wild-type; n = 18 neurons for R1117X^{+/+} from three pairs of littermates at 7 week's age.

(D–F) Typical NMDA receptors mediated currents from striatal MSNs by stimulating corpus callosum and quantification. n = 14 neurons for wild-type; n = 12 neurons for InsG3680^{+/+} from three pairs of littermates at 8 week's age. In both (C) and (F), data are presented as mean ± SEM. *p < 0.05; two-way ANOVA test.

were observed among all genotypes as indicated by similar NP1 response among genotypes (Figures 3C and 3F).

We further measured the AMPA receptor-mediated mEPSCs by performing whole-cell patch-clamping recordings on dorso-lateral striatal MSNs. We found that MSNs of both InsG3680 homozygous and heterozygous mice showed significant reduction of mEPSC frequency (Figures 3G and 3H). This reduction of mEPSC frequency was also observed in R1117X homozygous mice (Figures 3J and 3K). There is also a small but statistically significant reduction of mEPSC amplitude in MSNs from InsG3680^{+/+} and R1117X^{+/+} homozygous as well as R1117X^{+/−} mice (Figures 3I and 3L). In addition, we found significantly reduced NMDA receptor-mediated currents in both R1117X^{+/+} and InsG3680^{+/+} as compared to their wild-type controls (Figure 4). Together, these results suggest that both InsG3680 and R1117X mutations cause significant synaptic dysfunction in the adult striatum.

Distinct Alteration of Synaptic Transmission in Prefrontal Cortex of R1117X Mutant Mice

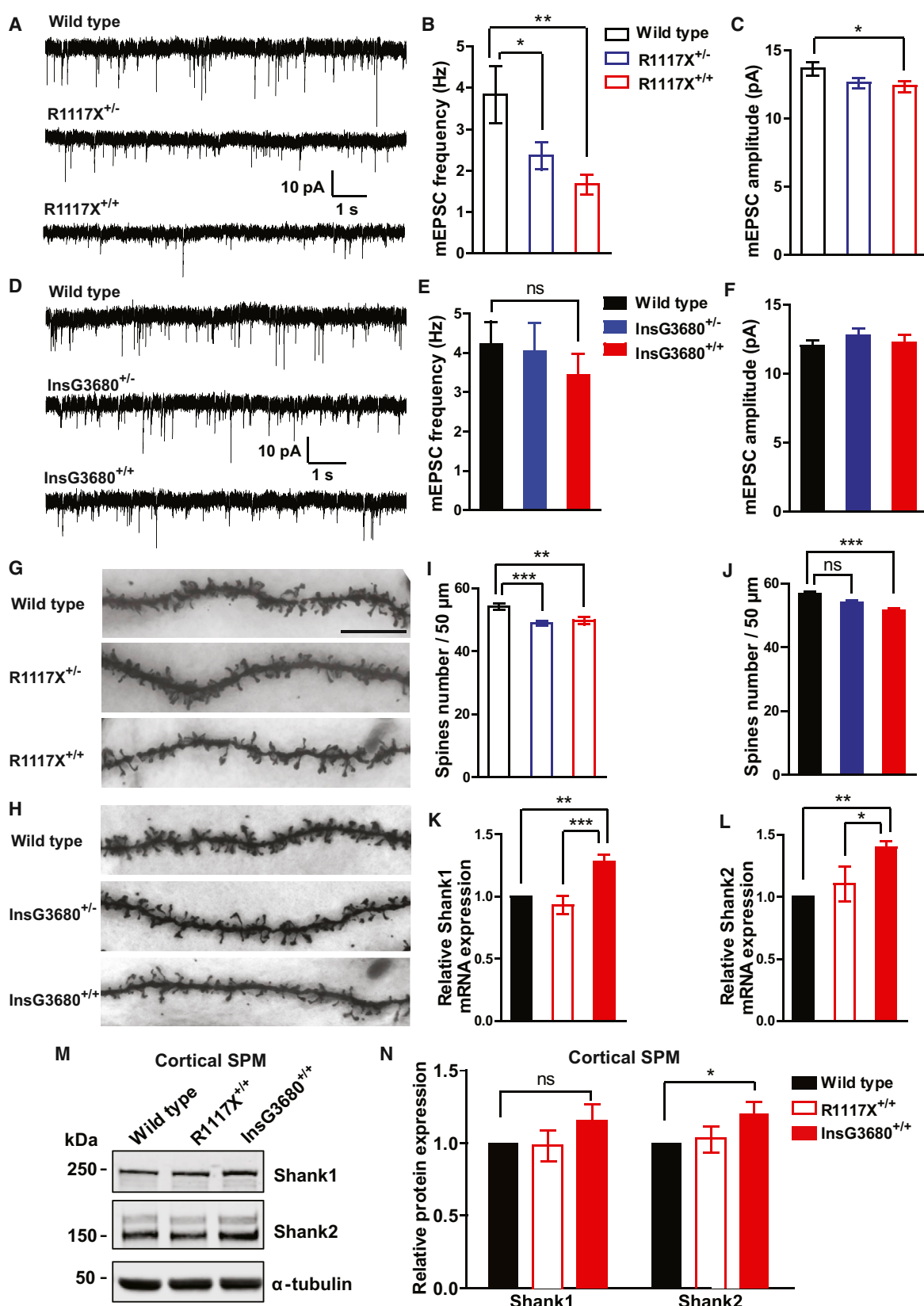
Although pathological mechanisms of schizophrenia are still not known, numerous patient studies have implicated the dysfunction of prefrontal cortex (PFC) as an important pathogenic source in patients (Anderson et al., 1999). We found a significant reduction of mEPSC frequency in pyramidal neurons of mPFC in both R1117X^{+/−} and R1117X^{+/+} mutant mice (Figures 5A and 5B). In addition, we observed a significant reduction of mEPSC amplitude in R1117X^{+/+} mice (Figure 5C). In contrast, no significant differences of either frequency or amplitude of mEPSC were

found in InsG3680^{+/−} or InsG3680^{+/+} mutant mice when compared to WT controls (Figures 5D–F), although there is a trend of reduction in mEPSC frequency in InsG3680^{+/+} mutant mice. These results indicate that the R1117X mutation, but not the InsG3680 mutation, causes a profound deficit of synaptic transmission in mPFC.

One of the pathological findings in postmortem brains of schizophrenia patients is the reduction of spine density of

layer 3 pyramidal neurons in the prefrontal cortex (Glantz and Lewis, 2000). To examine whether a similar defect exists in the two lines of *Shank3* mutant mice, we used Golgi staining to measure the spine density of layer 2/3 pyramidal neurons in the frontal association area. We found a significant reduction of spine density in both R1117X heterozygous and homozygous mutant mice (Figures 5G and 5I). We also found a significant reduction of spine density in InsG3680 homozygous but not heterozygous mutant mice (Figures 5H and 5J).

All three SHANK family members are highly homologous and expressed in the cortex (Böckers et al., 2004; Lim et al., 1999; Peça et al., 2011). It has been reported that SHANK3 was upregulated in *Shank2* knockout mice (Schmeisser et al., 2012). Thus, it is possible that SHANK1-2 may be upregulated in *Shank3* mutants to compensate for the loss of SHANK3. To explore this possibility, we quantified the expression level of *Shank1* and *Shank2* mRNA in the cortex of InsG3680^{+/+} and R1117X^{+/+} mutant mice. We found both *Shank1* and *Shank2* mRNAs were significantly upregulated in InsG3680^{+/+} but not R1117X^{+/+} mutant mice (Figures 5K and 5L), suggesting that the two mutations have differential effects on *Shank1* and *Shank2* mRNA upregulation. Furthermore, we observed significantly upregulated SHANK2 protein and a trend of increased SHANK1 protein in the cortex of InsG3680^{+/+} but not R1117X^{+/+} mutant mice (Figures 5M and 5N). However, we did not observe upregulation of either mRNA or protein of *Shank1* or *Shank2* in the striatum of either mutant line. Together, these results suggest both mutation-specific and circuit-specific upregulation of other Shank family members, and the upregulation of SHANK1 and SHANK2



(legend on next page)

mRNAs and proteins in the cortex of *InsG3680^{+/+}* mutant mice may partially compensate for the loss of *SHANK3* protein and thus alleviate synaptic defects in mPFC of *InsG3680^{+/+}* mutant mice.

Given the fact that patients carrying the schizophrenia-associated *R1117X* *Shank3* mutation were diagnosed at their late adolescence stage (Gauthier et al., 2010), we examined whether there are synaptic defects in the mPFC of young mice (P14) from either mutant line. Similar to our findings in the mEPSC of adult *InsG3680^{+/+}* mice, we did not detect significant differences of either mEPSC frequency or amplitude in the mPFC of P14 *InsG3680^{+/+}* mice (Figures S4D–S4F). Interestingly, we detected a significant increase in mEPSC frequency in *R1117X^{+/+}* mice at P14 (Figures S4A–S4C), suggesting there is already some degree of aberrant synaptic connection/function in the mPFC region at this age, albeit different from adult defects.

We next examined synaptic protein expression in cortical SPM preparations at P14. As shown in Figure S4, we did not detect significant changes in synaptic protein levels except a small reduction of Homer protein in *R1117X^{+/+}* mice (Figure S4H). Interestingly, we observed a significant upregulation of Shank2 protein in *InsG3680^{+/+}* mice (Figure S4H), which we also observed in adult cortical SPM preparations of *InsG3680^{+/+}* mice (Figures 5M and 5N). Together, these data indicate much minor molecular defects at cortical synapses at P14 in both lines.

Alteration of PSD Composition in Adult *R1117X* and *InsG3680* Mutant Mice

The PSD95-SAPAP-SHANK scaffolding complex has been proposed to play important roles in the trafficking, assembly, and anchoring of signaling proteins to the PSD as well as in regulating the dynamic plasticity of the PSD (Sheng and Kim, 2011). Our previous studies showed that several scaffolding proteins and glutamate receptor subunits were reduced in the striatal PSD of *Shank3B* knockout mice (Peça et al., 2011). Here we examined levels of several scaffolding and signaling proteins as well as glutamate receptor subunits in the SPM of *InsG3680^{+/+}* and *R1117X^{+/+}* mutant mice. In an SPM preparation from striatal

tissue, we found that Homer1b/c is dramatically reduced in both *InsG3680^{+/+}* and *R1117X^{+/+}* mutant mice (~14% of WT; Figures 6A and 6B). This is consistent with the fact that the Homer binding domain of *Shank3* is located downstream of the premature stop codons caused by *InsG3680* and *R1117X* mutation (Tu et al., 1999). Interestingly, we found that in *InsG3680* and *R1117X* heterozygous mice, which has about 50% of full-length *Shank3* protein, Homer protein is also reduced to 50% of the wild-type level (Figure S5), indicating the dependence of Homer synaptic localization on *Shank3* and their one-to-one stoichiometry.

In general, we observed a very similar pattern of reduced synaptic protein in the striatal SPM of the two mutant lines. SynGAP1, PSD95, SAPAP3, NR1, NR2A, NR2B, and GluR2 are all either significantly reduced or have the similar trend of reduction in both mutant lines (Figures 6A–6C). However, a small reduction of mGluR5 protein was only observed in the *InsG3680^{+/+}* line (Figures 6A and 6C). This correlates with the trend for impaired LTD maintenance 15~25 min after DHPG application compared to wild-type (Figure S6D) and mildly impaired PPR increase after DHPG-LTD in *InsG3680^{+/+}* (Figures S6G and S6H) but not *R1117X^{+/+}* mice (Figures S6C, S6E, and S6F). These data are consistent with our electrophysiological results showing severe striatal synaptic defects in adults of both mutant lines.

In the cortex, we found that Homer1b/c, PSD 95, and PSD 93 were significantly reduced in both *InsG3680^{+/+}* and *R1117X^{+/+}* mutant mice as compared to WT controls (Figures 6D and 6E). Interestingly, the level of Homer1b/c reduction is slightly more significant in *R1117X^{+/+}* mutant mice than in *InsG3680^{+/+}* mice (Figure 6E). In addition, we observed significant reduction of NR1 and its close interacting partner SynGAP1 only in the *R1117X^{+/+}* mutant mice (Figures 6D–6F), in line with previous findings using postmortem cortex tissue from schizophrenia patients (Funk et al., 2009; Weickert et al., 2013). Together, these data indicate that although cortical synaptic transmission defects are very different in the adults of the two mutant lines, differences in molecular defects are not as dramatic, raising the possibility that developmental defects in connectivity may contribute significantly to observed synaptic transmission and behavioral defects.

Figure 5. Profound Cortical Synaptic Defects Manifest in Mice Carrying the Schizophrenia-Associated *R1117X* Mutation

(A–C) Typical AMPA receptor-mediated mEPSC recordings in the prefrontal cortex and statistical results for *R1117X* mice. n = 13 neurons for WT; n = 20 neurons for *R1117X^{-/-}*; n = 18 neurons for *R1117X^{+/+}* from three pairs of mice. Note the highly significant reduction of mEPSC frequency in both heterozygous and homozygous mice and a modest reduction of amplitude in homozygotes.

(D–F) Typical AMPA receptor-mediated mEPSC recordings in the prefrontal cortex and statistical results for *InsG3680* cohort. n = 18 neurons for WT; n = 16 neurons for *InsG3680^{-/-}*; n = 17 neurons for *InsG3680^{+/+}* from three pairs of mice. Both heterozygous and homozygous mice display comparable miniature events to wild-type mice.

In (B), (C), (E), and (F), data are presented as mean ± SEM. *p < 0.05, **p < 0.01; one-way ANOVA with Bonferroni post hoc test.

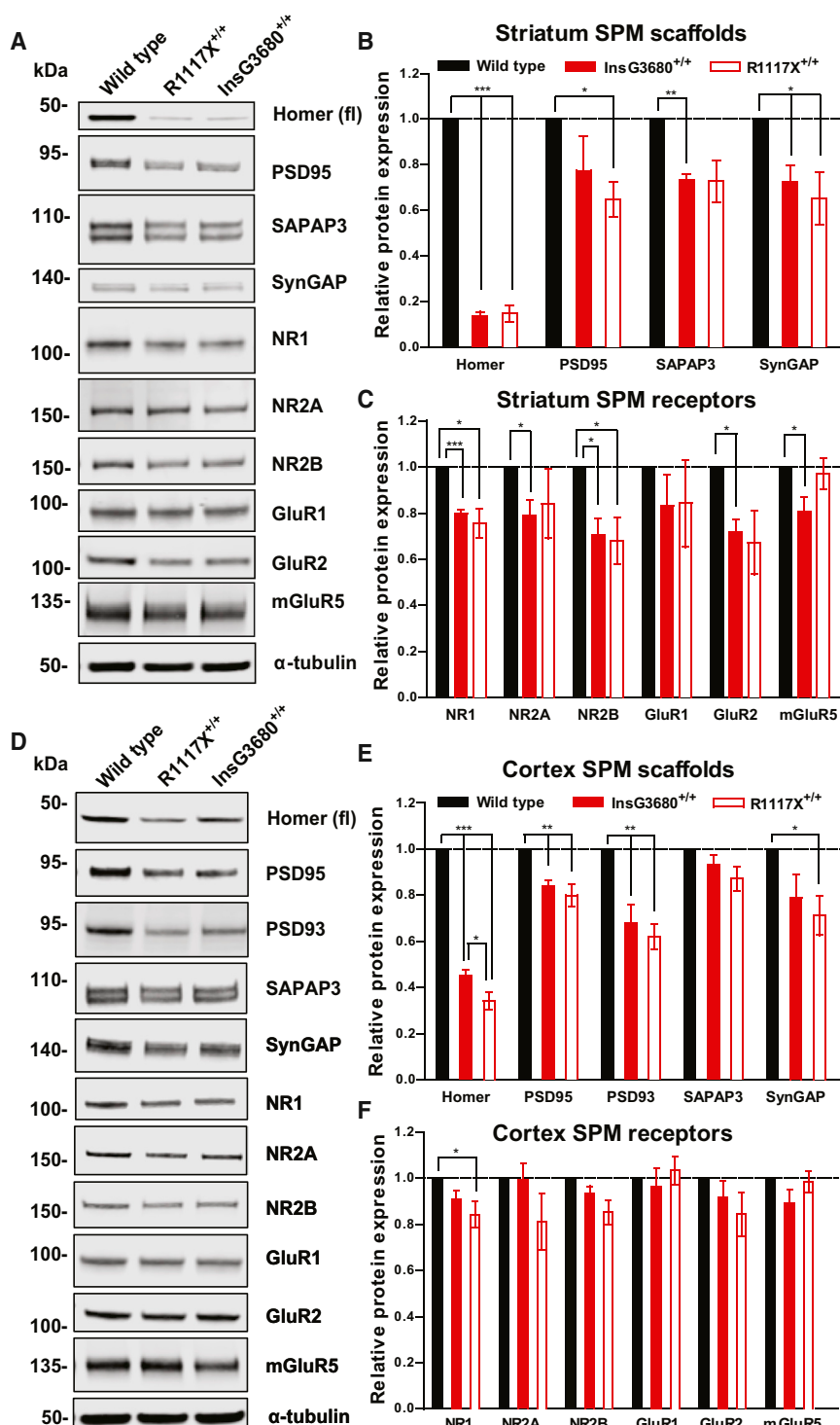
(G and H) Representative confocal images of secondary dendrites of pyramidal neurons from frontal association area of mice with indicated genotypes (scale bar, 10 μm).

(I and J) Quantification of spine number from neurons with indicated genotypes from three littermate pairs indicates reduced spine numbers in *R1117X^{-/-}*, *R1117X^{+/+}*, and *InsG3680^{+/+}* mice.

(K and L) mRNAs of *Shank3* homologs *Shank1* and *Shank2* are upregulated in cortical tissue from *InsG3680^{+/+}* compared to wild-type mice. Data are normalized to *Gapdh* mRNA and presented as mean ± SEM. WT mice (n = 5), *R1117X^{+/+}* mice (n = 5), and *InsG3680^{+/+}* mice (n = 5). In all the panels, data were collected from 2-month-old mice. In (I), (J), (K), and (L), *p < 0.05, **p < 0.01, ***p < 0.001; one-way ANOVA with Bonferroni post hoc test.

(M) Representative blots for proteins detected by specific antibodies in the cortical SPM fraction from adult wild-type, *R1117X^{+/+}*, and *InsG3680^{+/+}* mice.

(N) Adult *InsG3680^{+/+}* but not *R1117X^{+/+}* mice show increased Shank2 expression in cortical tissue. Quantification of relative levels of proteins as normalized to tubulin from cortical SPM. Data are presented as mean ± SEM *p < 0.05; one sample t test. (n = 8 samples per protein per genotype, each n being pooled tissue from two mice).



InsG3680 and R1117X Mutant Mice Show Both Common and Differential Behavioral Phenotypes

As described above, our molecular and electrophysiological studies of InsG3680 and R1117X mutant mice showed that they have both shared and distinct synaptic defects. We next

Figure 6. InsG3680 and R1117X Mutant Mice Display Common and Differential Disruptions of Post-synaptic Signaling Complexes

(A) Representative blots for proteins detected by specific antibodies in the striatal SPM fraction from wild-type, InsG3680^{+/+}, and R1117X^{+/+} mice.

(B and C) Quantification of relative levels of proteins as normalized to tubulin protein expression from striatal SPM. (n = 4–6 samples per protein per genotype, each n being pooled tissue from three mice).

(D) Representative blots for proteins detected by specific antibodies in the cortical SPM fraction from wild-type, InsG3680^{+/+}, and R1117X^{+/+} mice.

(E and F) Quantification of relative levels of proteins as normalized to tubulin protein expression from cortex SPM. (n = 4–11 samples per protein per genotype, each n being pooled tissue from two mice).

In (B), (C), (E), and (F), data are presented as mean ± SEM. *p < 0.05, **p < 0.01, ***p < 0.001; one sample t test.

tested whether these synaptic defects are accompanied by behavioral changes. We found that both R1117X^{+/+} and InsG3680^{+/+} mice show significantly reduced explorative activity in an open field arena (total distance) when compared to wild-type littermates (Figures 7A and 7B). In addition, InsG3680^{+/−} mice also showed significantly reduced activity (Figure 7A). Both lines of mutant mice show a very similar habituation time course compared to their wild-type littermates (Figures S7A and S7B), suggesting that the reduced explorative activity is caused by reduced locomotion rather than faster habituation of mutant mice. These reduced locomotion and hypoactive features in mutant mice were further supported by rotarod test findings showing that both R1117X^{+/+} and InsG3680^{+/+} *Shank3* mice have impaired motor learning and coordination capability (Figures S8A and S8B).

In addition to the hypoactive phenotype, both R1117X and InsG3680 *Shank3* mutant mice spent much less time exploring the center in an open area test compared to wild-type littermates (Figures S7C and S7D), suggesting an anxiety-like behavior. In the elevated zero

maze test, we found that both R1117X^{+/+} and InsG3680^{+/+} mice spent much less time in the open arms as compared to their wild-type littermates (Figures 7C and 7D). In addition, heterozygous mutants from both lines also spent less time in the open arms as compared to their wild-type littermates (Figures 7C

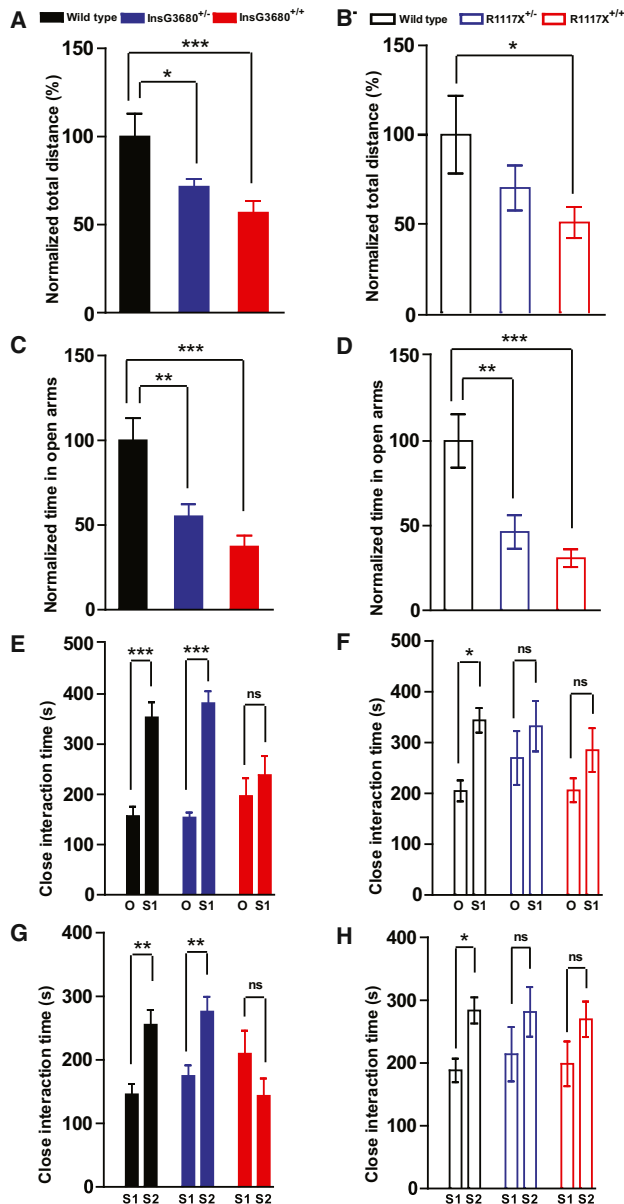


Figure 7. InsG3680 and R1117X Mutant Mice Display Anxiety Behavior and Social Interaction Deficits

(A and B) Total distance traveled in the open field test as normalized to wild-type littermates.
 (C and D) Time spent in the open arms in the elevated zero maze test as normalized to wild-type littermates.
 In the InsG3680 cohort, n = 17 mice for wild-type; n = 19 mice for InsG3680^{+/-}; n = 18 mice for InsG3680^{+/-} group. In the R1117X cohort, n = 15 mice for wild-type, n = 15 mice for R1117X^{+/-}; n = 15 mice for R1117X^{+/-}.
 (E and F) Time spent on close interaction with an object (O) versus stranger mice (S1) in the phase II social interaction test.
 (G and H) Time spent on close interaction with a familiar mouse (S1) versus stranger mouse (S2) in the phase III social interaction test.
 In the InsG3680 cohort, n = 17 mice for wild-type; n = 19 mice for InsG3680^{+/-}; n = 18 mice for InsG3680^{+/-} group; in the R1117X cohort, n = 23 for wild-type, n = 25 for R1117X^{+/-}; n = 24 for R1117X^{+/-} group.
 In all the panels, data are presented as mean ± SEM, *p < 0.05, **p < 0.01, ***p < 0.001; one-way ANOVA with Bonferroni post hoc test.

and 7D). These results indicate that both R1117X and InsG3680G mutant mice exhibit increased levels of anxiety.

Pre-pulse inhibition (PPI) is commonly used to test sensory-motor gating function in animal models of schizophrenia, although defects in PPI are not specific to schizophrenia and are present in many other psychiatric disorders, both in patients and animal models (Swerdlow et al., 1993; Joober et al., 2002). We found that both R1117X^{+/-} and InsG3680^{+/-} mice show profound defects in acoustic startle response (Figures S8C and S8D). Thus, although we found significantly reduced PPI in InsG3680^{+/-} and slightly impaired PPI in R1117X^{+/-} mice (Figures S8E and S8F), the interpretation of these data is complicated by the significant defects in startle response, because any PPI results are primarily confounded by a decrease in absolute startle to a 120 dB auditory stimulus. In addition, we found no difference in performance in the T maze spontaneous alternation test between wild-type and either line of mutant mice, suggesting normal basic working memory in both lines of mutant mice.

Since impaired social interaction is one of the core features of ASD patients and social withdraw is a characteristic negative symptom in schizophrenia patients, we tested social interactions of R1117X and InsG3680 mutant mice with a slightly modified standard three chamber social interaction paradigm (Chao et al., 2010; Silverman et al., 2010). As expected, wild-type mice showed significant preference for strange mouse (S1) to a novel object (O) (Figures 7E and 7F). However, both InsG3680 and R1117X homozygous mutant mice showed no significant preference for other mice compared to the novel object side (Figures 7E and 7F). Interestingly, heterozygous R1117X mutant mice, but not heterozygous InsG3680 mutant mice, also displayed social interaction deficits (Figure 7F). Similarly, in the social novelty test, both homozygous and heterozygous R1117X mutant mice exhibited deficits, while only homozygous InsG3680 mutant mice showed the defect (Figures 7G and 7H). Together, these results demonstrated that both the InsG3680 mutation and R1117X mutation lead to social interaction deficits, similar to *Shank3* mutant mice with deletion of either the ankyrin repeats or PDZ domain (Peça et al., 2011; Wang et al., 2011b).

Repetitive behavior/restricted interest is another key feature of ASD. Several mouse models of psychiatric disorders including ASD, OCD, and Tourette syndrome show repetitive grooming phenotypes and some of them develop skin lesions due to over-grooming (Karayannis et al., 2014; Peça et al., 2011; Rothwell et al., 2014; Welch et al., 2007). These repetitive/compulsive-like behaviors have been strongly linked to cortico-striatal-thalamo-cortical circuitry dysfunction (Ahmari et al., 2013; Burguière et al., 2013; Peça et al., 2011; Rothwell et al., 2014; Shmelkov et al., 2010; Welch et al., 2007). In our breeding colony, we found that 28.1% (18/64) of InsG3680^{+/-} mice develop lesions between 4 and 6 months of age (Figure 8A), a similar rate to our previous finding in *Shank3B* knockout mice (Peça et al., 2011). In contrast, only 8.7% (6/69) of R1117X^{+/-} mice developed skin lesions at the same age. Statistical analysis of lesion penetrance using chi-square test revealed significant difference between R1117X^{+/-} and InsG3680^{+/-} mice ($p = 0.0036$). No skin lesions were found in R1117X^{+/-}, InsG3680^{+/-} and wild-type groups. We next quantified the percentage of time R1117X and InsG3680 mice spent on grooming during a 2-hr session. We

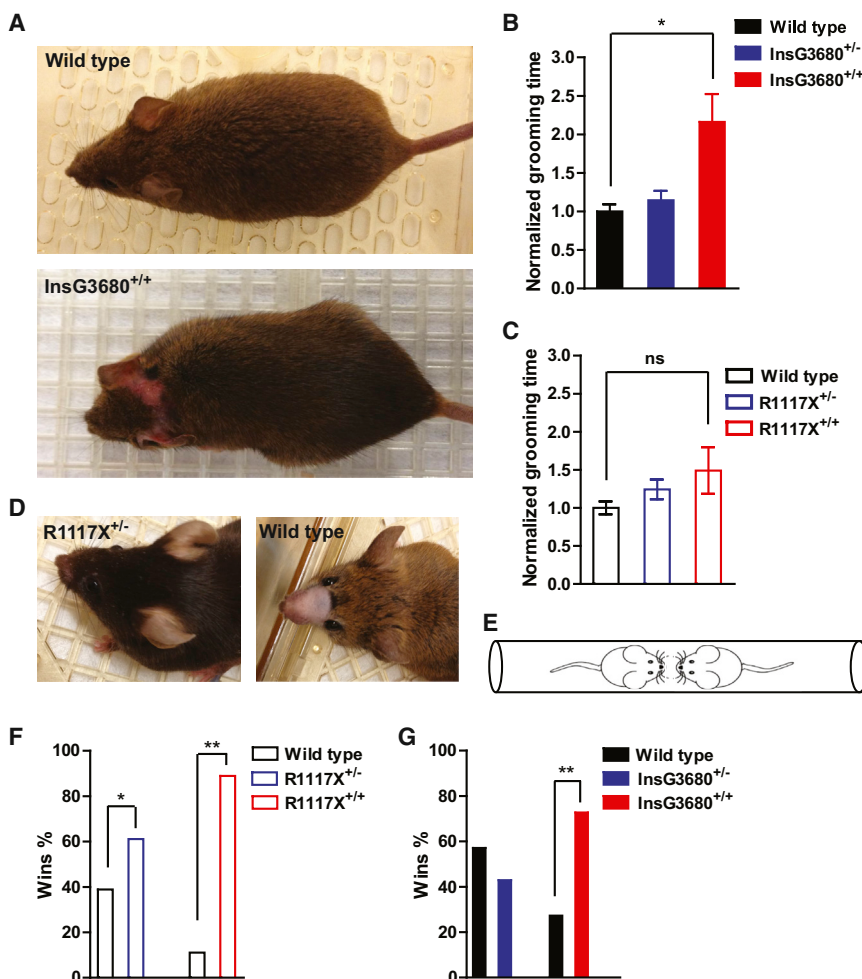


Figure 8. InsG3680 Mice Show More Profound Repetitive Self-Grooming, whereas R1117X Mice Display Allogrooming and Dominance-like Behavior

(A) Representative pictures from an adult wild-type and an InsG3680^{+/-} mouse that developed a lesion in the head/neck area.

(B and C) Time spent on grooming during 2 hr videotaping of indicated genotypes as normalized to their wild-type littermates. In the InsG3680 cohort, n = 9 mice for wild-type; n = 9 mice for InsG3680^{+/-}; n = 10 mice from InsG3680^{+/+} group. In the R1117X cohort, n = 9 mice for wild-type, n = 9 mice for R1117X^{+/-}; n = 9 mice for R1117X^{+/+}. Data are presented as mean \pm SEM. *p < 0.05; Kruskal-Wallis test with Dunn's post hoc comparison.

(D) Representative pictures of an R1117X^{+/-} mouse with intact facial hair and a wild-type mouse shaved by its cage mate as an indication for allogrooming behavior.

(E) Diagram of tube test task between two unfamiliar mice with different genotypes.

(F and G) Percentage of wins in test pairs between indicated genotypes, 11/18 (61%) of R1117X^{+/-} versus WT; 16/18 (89%) of R1117X^{+/+} versus WT; 6/14 (43%) of InsG3680^{+/-} versus WT; 8/11 (73%) of InsG3680^{+/+} versus WT. Note that both R1117X^{+/-} and R1117X^{+/+} mice perform significantly above chance level. One-sample chi-square test was used to determine the significant difference. ** indicates significantly different from an expected chance (50:50 win-lose outcome).

found that InsG3680^{+/+} mice spend twice as much time on grooming when compared to their WT littermates (Figure 8B), and a similar degree of increase in grooming time was also observed during the social interaction test. In contrast, R1117X^{+/+} mice did not show a statistically significant increase in grooming time compared to their WT littermates (Figure 8C), although a trend of increase was observed. These results suggest that only InsG3680^{+/+} mice show robust repetitive/compulsive grooming behavior.

In our R1117X^{+/-} × WT mating cages, we frequently observed partial or complete facial hair loss of WT mice without any lesions, suggesting allogrooming/barbering by R1117X^{+/-} mice (Figure 8D). We confirmed that loss of whisker and facial hair was caused by allogrooming by a cage mate instead of self-grooming by separating the mating pairs with the phenotype. We observed nearly full regrowth of facial hairs after weeks of single housing. Furthermore, pairing the recovered animals with their original cagemates induced robust loss of whisker and facial hair again within 2 weeks (data not shown). This allogrooming/barbering phenotype also occurred in R1117X^{+/-} × R1117X^{+/-} mating cages, in which one of the R1117X^{+/-} mice and/or offspring would lose their facial hair. We observed allogrooming/barbering in 48% (14 of 29) mating cages with R1117X^{+/-} mice. In contrast, we only observed allogrooming/barbering phenotype in 14% (5 of 37) mating cages with InsG3680^{+/-} mice.

Analysis of allogrooming phenotype penetrance using chi-square test revealed a significant difference between R1117X^{+/-} and InsG3680^{+/-} mice ($p = 0.002$). These results suggest that R1117X and InsG3680 mutations have differential effects on the expression of allogrooming/barbering phenotype.

Previous studies in rodents have implicated the impairment of PFC function in allogrooming/social dominance (Jiang-Xie et al., 2014; Wang et al., 2011a). Our electrophysiological findings from mPFC indicated that both R1117X^{+/-} and R1117X^{+/+} have profound deficits of synaptic transmission (Figures 5A–5C). To further evaluate the social dominance phenotype, we performed standard tube test (Figure 8E) between wild-type versus heterozygous and wild-type versus homozygous mice in the two mutant lines. When the two stranger mice meet in the middle of the tube, the dominant mouse will advance and drive the other mouse out of the tube (Wang et al., 2011a). We found that both R1117X^{+/-} and R1117X^{+/-} mice show much higher probability of winning the matches when tested with their wild-type opponents (Figure 8F). We also observed a significantly increased winning percentage in InsG3680^{+/+} but not in InsG3680^{+/-} mice against their wild-type opponents (Figure 8G). These results are consistent with our electrophysiological and

morphological findings in the prefrontal cortex showing synaptic deficits in both heterozygous and homozygous mice with R1117X mutation but only in homozygous mice with InsG3680 mutation.

DISCUSSION

Although schizophrenia and autism are two differential disorders based on phenomenological diagnosis (DSM-5), it has long been recognized that they share some common features and comorbidity (de Lacy and King, 2013; King and Lord, 2011). This is particularly true between child onset schizophrenia and autism (Meyer et al., 2011; Rapoport et al., 2009). For example, in a recent study, out of 46 schizophrenia patients with normal intelligence, about 50% met the diagnostic criteria of ASD (Unenge Hallerbäck et al., 2012). Recent human genetic studies have provided strong biological support for these clinical findings. GWAS, CNV, and exome sequencing have all identified many of the same genes in both disorders (Lee et al., 2013; Cross-Disorder Group of the Psychiatric Genomics Consortium, 2013; Krystal and State, 2014). Despite strong clinical and genetic evidence, however, it is not clear how different mutations of the same gene may contribute to different disorders. In this study, we generated new mouse models that harbor the highly penetrant *SHANK3* mutations found in ASD and schizophrenia patients. Our study revealed both distinct and shared defects in the two lines of mutant mice at molecular, synaptic, circuit, and behavioral levels (summarized in Table S2). Our results may provide, for the first time, some neurobiological insights on how different mutations in the *SHANK3* gene may lead to mutation-specific defects and relevant behavior abnormalities.

Early Synaptic Transmission Defects in the Striatum of Mice with ASD-Associated Mutation

One of our interesting findings is that mice with the ASD-associated InsG3680 mutation exhibit earlier synaptic transmission defects when compared with mice with the schizophrenia-associated R1117X mutation. We found a reduction of population spike responses in P14 InsG3680^{+/+} mutant mice, indicating defects in evoked striatal synaptic transmission. The lack of obvious presynaptic defects suggests that there are fewer functional synapses in these mutant mice. Interestingly, we found a surprising increase of GluR1 protein and mEPSC amplitude in striatal MSNs from P14 InsG3680^{+/+} mutant mice. Along with the trend of upregulation of many other synaptic proteins (Shank2, SynGAP, NR1, and NR2) in the striatum of P14 InsG3680^{+/+} mutant mice, this may reflect a potential compensatory mechanism by the remaining functional synapses to counteract defects in evoked synaptic transmission.

A puzzling finding in P14 striatum of R1117X mutant mice is the reduction of PSD93, SynGAP, NR1, NR2A, and NR2B proteins but normal basic synaptic transmission including population spike responses, AMPA/NMDA ratio, mEPSC frequency, and amplitude. We do not have a clear answer regarding this discrepancy between the electrophysiological and biochemical findings. One possible explanation is that the remaining truncated R1117X Shank3 protein is partially functional in MSNs at this developmental stage, as suggested by our study in cultured neurons,

and its presence is sufficient to maintain a basic level of synaptic transmission. However, it is also highly possible that striatal synaptic transmission in R1117X^{+/+} mutant mice at P14 is already mildly dysregulated and more extensive studies may reveal defects of other synaptic parameters.

Distinct Prefrontal Cortex Defects in R1117X Mutant Mice

Currently, the pathological mechanisms underlying schizophrenia are not well understood. However, clinical studies from human patients have implicated the dysfunction of prefrontal cortex (PFC), in particular dorsolateral prefrontal cortex (dlPFC), as an important cause of deficits in working memory, executive function, and social impairment (Anderson et al., 1999; Euston et al., 2012). In addition, postmortem studies have revealed reduced numbers of dendritic spines in pyramidal neurons of dlPFC region from schizophrenia patients (Glantz and Lewis, 2000). Rodents do not have an anatomically distinct dlPFC (Uylings et al., 2003). However, electrophysiological and behavioral studies suggest that medial prefrontal cortex (mPFC) in rodents may perform some equivalent functions to primate dlPFC at a rudimentary level (Seamans et al., 2008), such as working memory, decision making, and social interaction (Adhikari et al., 2010; Amodio and Frith, 2006; Wang et al., 2011a). Consistent with these findings, our study revealed profound synaptic transmission defects in mPFC of mice with the schizophrenia-associated R1117X mutation, but not with the ASD-associated InsG3680 mutation, indicating that these two mutations affect distinct circuits.

Since all three members of the Shank family genes are expressed in the cortex (Böckers et al., 2004; Lim et al., 1999; Peça et al., 2011), it is possible that they may have functional redundancy to compensate for the loss of other members. Very interestingly, we found that upregulation of *Shank1* and *Shank2* happens only in the cortex of InsG3680 mutants but not in R1117X mutants. The upregulation of *Shank1-2* in the cortex of InsG3680 mutants may compensate for the loss of *SHANK3* and thus alleviate synaptic defects. In addition, the truncated *SHANK3* protein resulting from the R1117X mutation may have a dominant-negative effect, preventing *SHANK1* and/or *SHANK2*, expressed at normal level, from assembling into the postsynaptic signaling complex. Such a dominant-negative effect would prevent compensation by *Shank1* and *Shank2* in R1117X mutants. Interestingly, *Shank1* and *Shank2* are normally not highly expressed in the striatum (Peça et al., 2011) and we did not observe upregulation of *Shank1* and *Shank2* in the striatum of either mutant line. Thus, upregulation and compensation by *Shank1* and *Shank2* is not only mutation specific, but also cell type/brain region specific, adding another layer of complexity to the study of neurobiological mechanisms underlying genetically overlapping psychiatric disorders.

Commonality and Differences in Behavioral Phenotypes

One of the most common phenotypes in mouse models with mutations of ASD risk genes is repetitive behavior, and previous studies have strongly linked repetitive/compulsive behaviors to defects in cortico-striatal-thalamo-cortical (CSTC) circuits (Burguière et al., 2013; Peça et al., 2011; Rothwell et al., 2014;

Shmelkov et al., 2010; Welch et al., 2007). Similar to our reported *Shank3B* knockout mice, the repetitive/compulsive grooming behaviors in InsG3680 mutant mice are very robust. R1117X mutant mice do not show significant repetitive grooming behavior, although both mutant lines show striatal molecular and synaptic defects. There are several possible explanations for this phenotypic difference. First of all, the striatum is only one part of the CTC circuit, and differential defects in other parts of the brain, such as the cortex, may significantly affect the behavioral output. Second, recent studies have begun to reveal specific changes in subcircuits/microcircuits of the CTC that may underlie repetitive behaviors, and the two mutations may differentially affect these sub-circuits/micro-circuits. Finally and probably most importantly, striatal synaptic transmission defects at early developmental stages in InsG3680 mutants may lead to long-lasting alterations in striatal connectivity. These connectivity defects may lead to InsG3680-specific circuit dysfunction and overgrooming even though synaptic transmission defects are similar between the two mutant lines in adults.

A behavioral phenotype predominantly found in R1117X mutants is the allogrooming and social dominance behavior. Although the exact mechanisms/circuits involved in dominance behaviors in mice are still not well understood, recent studies have provided evidence implicating mPFC in social dominance (Lin et al., 2011; Wang et al., 2014a). Our studies demonstrated significant synaptic transmission defects in the mPFC of R1117X, but not InsG3680 mutant mice. These correlative data may provide a partial explanation for the difference in social dominance behavior between these two mutant lines.

Previous studies have demonstrated that two different mutations of the *MECP2* gene in Rett Syndrome patients differentially affect the function of a key domain in MeCP2 and result in different severity of phenotypes in mice similar to the disease progression and symptoms observed in patients with these two mutations (Baker et al., 2013). Although it is difficult to directly correlate mouse behaviors with patient symptoms and diagnosis, our study at least provides neurobiological evidences and mechanisms that the two *SHANK3* mutations associated with ASD and schizophrenia cause both common and differential defects at molecular, synaptic, and behavioral levels. More broadly, we demonstrated that different mutations of the same gene may elicit neurobiological changes at different developmental stages, brain regions, and cell types through a variety of potential mechanisms including differential mRNA stability, differential regulation of compensatory gene expression, and different degrees of signaling complex disruption. Thus, future detailed analysis of such mutations will help to gain a more precise understanding of synaptic development and function.

EXPERIMENTAL PROCEDURES

Animal Work Statement

All animal-related work was performed under the guidelines of Division of Comparative Medicine (DCM), with protocol (# 0513-044-16 of Feng laboratory and #1012-102-15 of Lewis laboratory) approved by Committee for Animal Care (CAC) of Massachusetts Institute of Technology and was consistent with the Guide for Care and Use of Laboratory Animals, National Research Council 1996 (institutional animal welfare assurance no. A-3125-01). Only aged-matched male mice were used for all behavioral experiments; all other

tests included age-matched males and females in proportional contribution across groups.

Behavioral Studies

All behavioral studies were carried out and analyzed with experimenter blinded to genotype. For all assays, mice were habituated in the test facility for 1 hr prior to starting the task. Each cohort of mice was used for maximally three behavioral tests with at least 5 days' break between tasks.

Electrophysiological Recordings

All electrophysiological measurements were performed and analyzed with experimenter blinded to genotype.

Data Analysis

All comparisons between groups were collected from littermate animals with experiments performed at the same time. All results were presented as mean \pm SEM and were analyzed statistically using Student's t test, one-way or two-way analysis of variance with proper post hoc test as specified in legend of each figure (GraphPad Prism, RRID: rid_000081, SCR_002798). * $p < 0.05$; ** $p < 0.01$; *** $p < 0.001$.

SUPPLEMENTAL INFORMATION

Supplemental Information includes Supplemental Experimental Procedures, eight figures, and one table and can be found with this article online at <http://dx.doi.org/10.1016/j.neuron.2015.11.023>.

AUTHOR CONTRIBUTIONS

Yang Z. and G.F. conceived the study. Yang Z., Yongdi Z., Mingjie Z., and G.F. designed the experiments and oversaw the project. Yang Z. generated the mutant mice. F.Z. and N.S. provided resource at the early stage of this project. T.K. and Yang Z. performed the biochemical studies of SPM/PSD and data analysis. Z.F., P.M., Yang Z., M.S.V.D.G., and Chenchen L. performed electrophysiological recording. D.W. imaged Golgi slices and analyzed the spine density. Congyi L. performed cultured neuron experiments. X.Z. and Yang Z. conducted the mRNA Q-PCR assay. Yang Z., X.Z., Menglong Z., D.W., B.B., A.A., S.N., M.L., and M.W. designed, performed and analyzed the behavioral experiments. Yang Z. and G.F. wrote the manuscript with inputs from all authors. Tobias Kaiser, Patricia Monteiro and Xiangyu Zhang contributed equally to this work.

ACKNOWLEDGMENTS

We thank Ms. Peimin Qi of MIT transgenic facility for support with ES cell injection, Ms. Elaine Kun, Heather Zaniewski and Ms. Triana Dalia for help with animal care and experiments, Alexandra Krol for critical reading of the manuscript and the Feng lab members for helpful discussion. We are also grateful to Dr. Paul Worley (Johns Hopkins University) for generous sharing their SHANK3 antibodies and Dr. Hailan Hu (Shanghai Institute of Neuroscience, Chinese Academy of Sciences) for advice on tube test assay. This work is supported by the Simons Center for the Social Brain at MIT and the Stanley Center for Psychiatric Research at Broad Institute. G.F. is supported by the National Institute of Mental Health (5R01MH097104), the Poitras Center for Affective Disorders Research at MIT, Stanley Center for Psychiatric Research at Broad Institute of MIT and Harvard, Nancy Lurie Marks Family Foundation, Simons Foundation Autism Research Initiative (SFARI), and Simons Center for the Social Brain at MIT. Additional support is provided by Robert Buxton, Marshall Tulin, and John and Valerie Stelling. Yang Zhou is supported by postdoc fellowships from the Simons Center for the Social Brain at MIT, Nancy Lurie Marks Family Foundation and Shenzhen Overseas Innovation Team Project (No. KQT20140630180249366). P.M. was supported by the Stanley Center for Psychiatric Research at the Broad Institute of MIT and Harvard and a doctoral fellowship from the Portuguese Foundation for Science and Technology (SFRH/BD/33894/2009). B.B. is supported by postdoc fellowships from the Simons Center for the Social Brain at MIT and the Autism Science

Foundation. Mingjie Zhang is supported by grants from Research Grant Council of Hong Kong (AoE/M09/12). Z.F. is supported by Stanley Center for Psychiatric Research at Broad Institute of MIT and Harvard and NARSAD Young Investigator Grant from the Brain & Behavior Research Foundation. T.K. is supported by the Leonardo Kolleg, the Dr. Ernst und Anita Bauer-Stiftung and the Henry E. Singleton Fellowship. F.Z. is supported by the NIMH through a NIH Director's Pioneer Award (DP1-MH100706), the NINDS through a NIH Transformative R01 grant (R01-NS 07312401), NSF Waterman Award, the Keck, Damon Runyon, Searle Scholars, Klingenstein, Vallee, Merkin, and Simons Foundations, and Bob Metcalfe.

Received: February 15, 2015

Revised: August 27, 2015

Accepted: November 2, 2015

Published: December 10, 2015

REFERENCES

- Adhikari, A., Topiwala, M.A., and Gordon, J.A. (2010). Synchronized activity between the ventral hippocampus and the medial prefrontal cortex during anxiety. *Neuron* 65, 257–269.
- Ahmari, S.E., Spellman, T., Douglass, N.L., Kheirbek, M.A., Simpson, H.B., Deisseroth, K., Gordon, J.A., and Hen, R. (2013). Repeated cortico-striatal stimulation generates persistent OCD-like behavior. *Science* 340, 1234–1239.
- Amadio, D.M., and Frith, C.D. (2006). Meeting of minds: the medial frontal cortex and social cognition. *Nat. Rev. Neurosci.* 7, 268–277.
- Anderson, S.W., Bechara, A., Damasio, H., Tranel, D., and Damasio, A.R. (1999). Impairment of social and moral behavior related to early damage in human prefrontal cortex. *Nat. Neurosci.* 2, 1032–1037.
- Baker, S.A., Chen, L., Wilkins, A.D., Yu, P., Lichtarge, O., and Zoghbi, H.Y. (2013). An AT-hook domain in MeCP2 determines the clinical course of Rett syndrome and related disorders. *Cell* 152, 984–996.
- Böckers, T.M., Segger-Junius, M., Iglauder, P., Bockmann, J., Gundelfinger, E.D., Kreutz, M.R., Richter, D., Kindler, S., and Kreienkamp, H.J. (2004). Differential expression and dendritic transcript localization of Shank family members: identification of a dendritic targeting element in the 3' untranslated region of Shank1 mRNA. *Mol. Cell. Neurosci.* 26, 182–190.
- Boeckers, T.M., Kreutz, M.R., Winter, C., Zuschratter, W., Smalla, K.H., Sanmarti-Vila, L., Wex, H., Langnaese, K., Bockmann, J., Garner, C.C., and Gundelfinger, E.D. (1999). Proline-rich synapse-associated protein-1/cortactin binding protein 1 (ProSAP1/CortBP1) is a PDZ-domain protein highly enriched in the postsynaptic density. *J. Neurosci.* 19, 6506–6518.
- Bonaglia, M.C., Giorda, R., Beri, S., De Agostini, C., Novara, F., Fichera, M., Grillo, L., Galesi, O., Vetro, A., Ciccone, R., et al. (2011). Molecular mechanisms generating and stabilizing terminal 22q13 deletions in 44 subjects with Phelan/McDermid syndrome. *PLoS Genet.* 7, e1002173.
- Bozdagi, O., Sakurai, T., Papapetrou, D., Wang, X., Dickstein, D.L., Takahashi, N., Kajiwara, Y., Yang, M., Katz, A.M., Scattoni, M.L., et al. (2010). Haploinsufficiency of the autism-associated *Shank3* gene leads to deficits in synaptic function, social interaction, and social communication. *Mol. Autism* 1, 15.
- Burguière, E., Monteiro, P., Feng, G., and Graybiel, A.M. (2013). Optogenetic stimulation of lateral orbitofronto-striatal pathway suppresses compulsive behaviors. *Science* 340, 1243–1246.
- Chao, H.T., Chen, H., Samaco, R.C., Xue, M., Chahrour, M., Yoo, J., Neul, J.L., Gong, S., Lu, H.C., Heintz, N., et al. (2010). Dysfunction in GABA signalling mediates autism-like stereotypies and Rett syndrome phenotypes. *Nature* 468, 263–269.
- Cross-Disorder Group of the Psychiatric Genomics Consortium (2013). Identification of risk loci with shared effects on five major psychiatric disorders: a genome-wide analysis. *Lancet* 381, 1371–1379.
- de Lacy, N., and King, B.H. (2013). Revisiting the relationship between autism and schizophrenia: toward an integrated neurobiology. *Annu. Rev. Clin. Psychol.* 9, 555–587.
- De Rubeis, S., He, X., Goldberg, A.P., Poultnay, C.S., Samocha, K., Cicek, A.E., Kou, Y., Liu, L., Fromer, M., Walker, S., et al.; DDD Study; Homozygosity Mapping Collaborative for Autism; UK10K Consortium (2014). Synaptic, transcriptional and chromatin genes disrupted in autism. *Nature* 515, 209–215.
- Durand, C.M., Betancur, C., Boeckers, T.M., Bockmann, J., Chaste, P., Fauchereau, F., Nygren, G., Rastam, M., Gillberg, I.C., Ankarsäter, H., et al. (2007). Mutations in the gene encoding the synaptic scaffolding protein SHANK3 are associated with autism spectrum disorders. *Nat. Genet.* 39, 25–27.
- Euston, D.R., Gruber, A.J., and McNaughton, B.L. (2012). The role of medial prefrontal cortex in memory and decision making. *Neuron* 76, 1057–1070.
- Frischmeyer, P.A., and Dietz, H.C. (1999). Nonsense-mediated mRNA decay in health and disease. *Hum. Mol. Genet.* 8, 1893–1900.
- Fromer, M., Pocklington, A.J., Kavanagh, D.H., Williams, H.J., Dwyer, S., Gormley, P., Georgieva, L., Rees, E., Palta, P., Ruderfer, D.M., et al. (2014). De novo mutations in schizophrenia implicate synaptic networks. *Nature* 506, 179–184.
- Funk, A.J., Rumbaugh, G., Haroutunian, V., McCullumsmith, R.E., and Meadow-Woodruff, J.H. (2009). Decreased expression of NMDA receptor-associated proteins in frontal cortex of elderly patients with schizophrenia. *Neuroreport* 20, 1019–1022.
- Gauthier, J., Spiegelman, D., Piton, A., Lafrenière, R.G., Laurent, S., St-Onge, J., Lapointe, L., Hamdan, F.F., Cossette, P., Mottron, L., et al. (2009). Novel de novo SHANK3 mutation in autistic patients. *Am. J. Med. Genet. B. Neuropsychiatr. Genet.* 150B, 421–424.
- Gauthier, J., Champagne, N., Lafrenière, R.G., Xiong, L., Spiegelman, D., Brustein, E., Lapointe, M., Peng, H., Côté, M., Noreau, A., et al.; S2D Team (2010). De novo mutations in the gene encoding the synaptic scaffolding protein SHANK3 in patients ascertained for schizophrenia. *Proc. Natl. Acad. Sci. USA* 107, 7863–7868.
- Glantz, L.A., and Lewis, D.A. (2000). Decreased dendritic spine density on prefrontal cortical pyramidal neurons in schizophrenia. *Arch. Gen. Psychiatry* 57, 65–73.
- Guilmatre, A., Huguet, G., Delorme, R., and Bourgeron, T. (2014). The emerging role of SHANK genes in neuropsychiatric disorders. *Dev. Neurobiol.* 74, 113–122.
- Han, K., Holder, J.L., Jr., Schaaf, C.P., Lu, H., Chen, H., Kang, H., Tang, J., Wu, Z., Hao, S., Cheung, S.W., et al. (2013). SHANK3 overexpression causes manic-like behaviour with unique pharmacogenetic properties. *Nature* 503, 72–77.
- Jiang-Xie, L.F., Liao, H.M., Chen, C.H., Chen, Y.T., Ho, S.Y., Lu, D.H., Lee, L.J., Liou, H.H., Fu, W.M., and Gau, S.S. (2014). Autism-associated gene Dlgap2 mutant mice demonstrate exacerbated aggressive behaviors and orbitofrontal cortex deficits. *Mol. Autism* 5, 32.
- Joober, R., Zarate, J.M., Rouleau, G.A., Skamene, E., and Boksa, P. (2002). Provisional mapping of quantitative trait loci modulating the acoustic startle response and prepulse inhibition of acoustic startle. *Neuropharmacology* 27, 765–781.
- Karayannis, T., Au, E., Patel, J.C., Kruglikov, I., Markx, S., Delorme, R., Héron, D., Salomon, D., Glessner, J., Restituito, S., et al. (2014). Cntnap4 differentially contributes to GABAergic and dopaminergic synaptic transmission. *Nature* 511, 236–240.
- Kenny, E.M., Cormican, P., Furlong, S., Heron, E., Kenny, G., Fahey, C., Kelleher, E., Ennis, S., Tropea, D., Anney, R., et al. (2014). Excess of rare novel loss-of-function variants in synaptic genes in schizophrenia and autism spectrum disorders. *Mol. Psychiatry* 19, 872–879.
- Kim, E., and Sheng, M. (2004). PDZ domain proteins of synapses. *Nat. Rev. Neurosci.* 5, 771–781.
- King, B.H., and Lord, C. (2011). Is schizophrenia on the autism spectrum? *Brain Res.* 1380, 34–41.
- Kouser, M., Speed, H.E., Dewey, C.M., Reimers, J.M., Widman, A.J., Gupta, N., Liu, S., Jaramillo, T.C., Bangash, M., Xiao, B., et al. (2013). Loss of

- predominant *Shank3* isoforms results in hippocampus-dependent impairments in behavior and synaptic transmission. *J. Neurosci.* 33, 18448–18468.
- Krystal, J.H., and State, M.W. (2014). Psychiatric disorders: diagnosis to therapy. *Cell* 157, 201–214.
- Lee, S.H., Ripke, S., Neale, B.M., Faraone, S.V., Purcell, S.M., Perlis, R.H., Mowry, B.J., Thapar, A., Goddard, M.E., Witte, J.S., et al.; Cross-Disorder Group of the Psychiatric Genomics Consortium; International Inflammatory Bowel Disease Genetics Consortium (IIBDGC) (2013). Genetic relationship between five psychiatric disorders estimated from genome-wide SNPs. *Nat. Genet.* 45, 984–994.
- Lim, S., Naisbitt, S., Yoon, J., Hwang, J.I., Suh, P.G., Sheng, M., and Kim, E. (1999). Characterization of the Shank family of synaptic proteins. Multiple genes, alternative splicing, and differential expression in brain and development. *J. Biol. Chem.* 274, 29510–29518.
- Lin, D., Boyle, M.P., Dollar, P., Lee, H., Lein, E.S., Perona, P., and Anderson, D.J. (2011). Functional identification of an aggression locus in the mouse hypothalamus. *Nature* 470, 221–226.
- McAllister, A.K. (2007). Dynamic aspects of CNS synapse formation. *Annu. Rev. Neurosci.* 30, 425–450.
- McCarthy, S.E., Gillis, J., Kramer, M., Lihm, J., Yoon, S., Bernstein, Y., Mistry, M., Pavlidis, P., Solomon, R., Ghiban, E., et al. (2014). De novo mutations in schizophrenia implicate chromatin remodeling and support a genetic overlap with autism and intellectual disability. *Mol. Psychiatry* 19, 652–658.
- Meyer, U., Feldon, J., and Dammann, O. (2011). Schizophrenia and autism: both shared and disorder-specific pathogenesis via perinatal inflammation? *Pediatr. Res.* 69, 26R–33R.
- Moessner, R., Marshall, C.R., Sutcliffe, J.S., Skaug, J., Pinto, D., Vincent, J.J., Zwaigenbaum, L., Fernandez, B., Roberts, W., Szatmari, P., and Scherer, S.W. (2007). Contribution of SHANK3 mutations to autism spectrum disorder. *Am. J. Hum. Genet.* 81, 1289–1297.
- Naisbitt, S., Kim, E., Tu, J.C., Xiao, B., Sala, C., Valtschanoff, J., Weinberg, R.J., Worley, P.F., and Sheng, M. (1999). Shank, a novel family of postsynaptic density proteins that binds to the NMDA receptor/PSD-95/GKAP complex and cortactin. *Neuron* 23, 569–582.
- Peça, J., Feliciano, C., Ting, J.T., Wang, W., Wells, M.F., Venkatraman, T.N., Lascola, C.D., Fu, Z., and Feng, G. (2011). Shank3 mutant mice display autistic-like behaviours and striatal dysfunction. *Nature* 472, 437–442.
- Rapoport, J., Chavez, A., Greenstein, D., Addington, A., and Gogtay, N. (2009). Autism spectrum disorders and childhood-onset schizophrenia: clinical and biological contributions to a relation revisited. *J. Am. Acad. Child Adolesc. Psychiatry* 48, 10–18.
- Rothwell, P.E., Fuccillo, M.V., Maxeiner, S., Hayton, S.J., Gokce, O., Lim, B.K., Fowler, S.C., Malenka, R.C., and Südhof, T.C. (2014). Autism-associated neuroligin-3 mutations commonly impair striatal circuits to boost repetitive behaviors. *Cell* 158, 198–212.
- Roussignol, G., Ango, F., Romorini, S., Tu, J.C., Sala, C., Worley, P.F., Bockaert, J., and Fagni, L. (2005). Shank expression is sufficient to induce functional dendritic spine synapses in aspiny neurons. *J. Neurosci.* 25, 3560–3570.
- Saal, D., Dong, Y., Bonci, A., and Malenka, R.C. (2003). Drugs of abuse and stress trigger a common synaptic adaptation in dopamine neurons. *Neuron* 37, 577–582.
- Sala, C., Piëch, V., Wilson, N.R., Passafaro, M., Liu, G., and Sheng, M. (2001). Regulation of dendritic spine morphology and synaptic function by Shank and Homer. *Neuron* 31, 115–130.
- Schizophrenia Working Group of the Psychiatric Genomics Consortium (2014). Biological insights from 108 schizophrenia-associated genetic loci. *Nature* 511, 421–427.
- Schmeisser, M.J., Ey, E., Wegener, S., Bockmann, J., Stempel, A.V., Kuebler, A., Janssen, A.L., Udvardi, P.T., Shiban, E., Spilker, C., et al. (2012). Autistic-like behaviours and hyperactivity in mice lacking ProSAP1/Shank2. *Nature* 486, 256–260.
- Seamans, J.K., Lapish, C.C., and Durstewitz, D. (2008). Comparing the pre-frontal cortex of rats and primates: insights from electrophysiology. *Neurotox. Res.* 14, 249–262.
- Sheng, M., and Kim, E. (2011). The postsynaptic organization of synapses. *Cold Spring Harb. Perspect. Biol.* 3, 3.
- Shmelkov, S.V., Hormigo, A., Jing, D., Proenca, C.C., Bath, K.G., Milde, T., Shmelkov, E., Kushner, J.S., Baljevic, M., Dincheva, I., et al. (2010). Slitrk5 deficiency impairs corticostratial circuitry and leads to obsessive-compulsive-like behaviors in mice. *Nat. Med.* 16, 598–602, 1p, 602.
- Silverman, J.L., Yang, M., Lord, C., and Crawley, J.N. (2010). Behavioural phenotyping assays for mouse models of autism. *Nat. Rev. Neurosci.* 11, 490–502.
- Swerdlow, N.R., Benbow, C.H., Zisook, S., Geyer, M.A., and Braff, D.L. (1993). A preliminary assessment of sensorimotor gating in patients with obsessive compulsive disorder. *Biol. Psychiatry* 33, 298–301.
- Tu, J.C., Xiao, B., Naisbitt, S., Yuan, J.P., Petralia, R.S., Brakeman, P., Doan, A., Aakalu, V.K., Lanahan, A.A., Sheng, M., and Worley, P.F. (1999). Coupling of mGluR/Homer and PSD-95 complexes by the Shank family of postsynaptic density proteins. *Neuron* 23, 583–592.
- Unenge Hallerbäck, M., Lugnegård, T., and Gillberg, C. (2012). Is autism spectrum disorder common in schizophrenia? *Psychiatry Res.* 198, 12–17.
- Uylings, H.B., Groenewegen, H.J., and Kolb, B. (2003). Do rats have a prefrontal cortex? *Behav. Brain Res.* 146, 3–17.
- Wang, F., Zhu, J., Zhu, H., Zhang, Q., Lin, Z., and Hu, H. (2011a). Bidirectional control of social hierarchy by synaptic efficacy in medial prefrontal cortex. *Science* 334, 693–697.
- Wang, X., McCoy, P.A., Rodriguez, R.M., Pan, Y., Je, H.S., Roberts, A.C., Kim, C.J., Berrios, J., Colvin, J.S., Bousquet-Moore, D., et al. (2011b). Synaptic dysfunction and abnormal behaviors in mice lacking major isoforms of Shank3. *Hum. Mol. Genet.* 20, 3093–3108.
- Wang, F., Kessels, H.W., and Hu, H. (2014a). The mouse that roared: neural mechanisms of social hierarchy. *Trends Neurosci.* 37, 674–682.
- Wang, X., Xu, Q., Bey, A.L., Lee, Y., and Jiang, Y.H. (2014b). Transcriptional and functional complexity of Shank3 provides a molecular framework to understand the phenotypic heterogeneity of SHANK3 causing autism and Shank3 mutant mice. *Mol. Autism* 5, 30.
- Weickert, C.S., Fung, S.J., Catts, V.S., Schofield, P.R., Allen, K.M., Moore, L.T., Newell, K.A., Pellen, D., Huang, X.F., Catts, S.V., and Weickert, T.W. (2013). Molecular evidence of N-methyl-D-aspartate receptor hypofunction in schizophrenia. *Mol. Psychiatry* 18, 1185–1192.
- Welch, J.M., Lu, J., Rodriguez, R.M., Trotta, N.C., Peça, J., Ding, J.D., Feliciano, C., Chen, M., Adams, J.P., Luo, J., et al. (2007). Cortico-striatal synaptic defects and OCD-like behaviours in Sapap3-mutant mice. *Nature* 448, 894–900.
- Wilson, H.L., Wong, A.C., Shaw, S.R., Tse, W.Y., Stapleton, G.A., Phelan, M.C., Hu, S., Marshall, J., and McDermid, H.E. (2003). Molecular characterisation of the 22q13 deletion syndrome supports the role of haploinsufficiency of SHANK3/PROSAP2 in the major neurological symptoms. *J. Med. Genet.* 40, 575–584.

Neuron

Supplemental Information

**Mice with *Shank3* Mutations Associated
with ASD and Schizophrenia Display
Both Shared and Distinct Defects**

**Yang Zhou, Tobias Kaiser, Patrícia Monteiro, Xiangyu Zhang, Marie. S. Van der Goes,,
Dongqing Wang, Boaz Barak, Menglong Zeng, Chenchen Li, Congyi Lu, Michael Wells,
Aldo Amaya, Shannon Nguyen, Michael Lewis, Neville Sanjana, Yongdi Zhou, Mingjie
Zhang, Feng Zhang, Zhanyan Fu, and Guoping Feng**

Fig S1

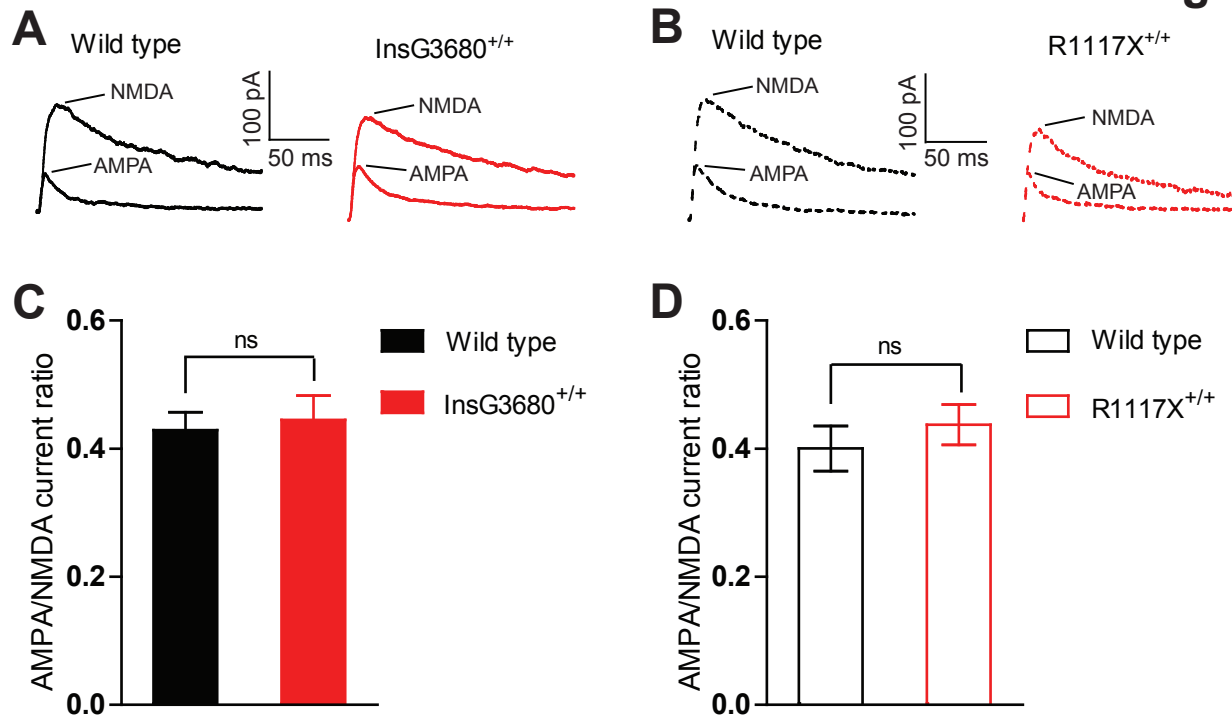


Fig S1. No change of AMPA to NMDA ratio in MSNs from *R1117X^{+/+}* and *InsG3680^{+/+}* at P14. Related to Figure 2.

(A and B) Representative AMPA current traces and digitally substracted NMDA current traces from striatal MSNs with indicated genotypes.

(C and D) No significant difference of AMPA to NMDA current ratio between *InsG3680^{+/+}*, *R1117X^{+/+}* mice and their wild type littermates. In *InsG3680* cohort, n = 14 neurons for wild type, n = 16 neurons for *InsG3680^{+/+}* from three pairs of littermates; in *R1117X* cohort, n = 18 neurons for wild type, n = 19 neurons for *R1117X^{+/+}* from three pairs of littermates. Data are presented as mean ± SEM; two-tailed student t-test.

Fig S2

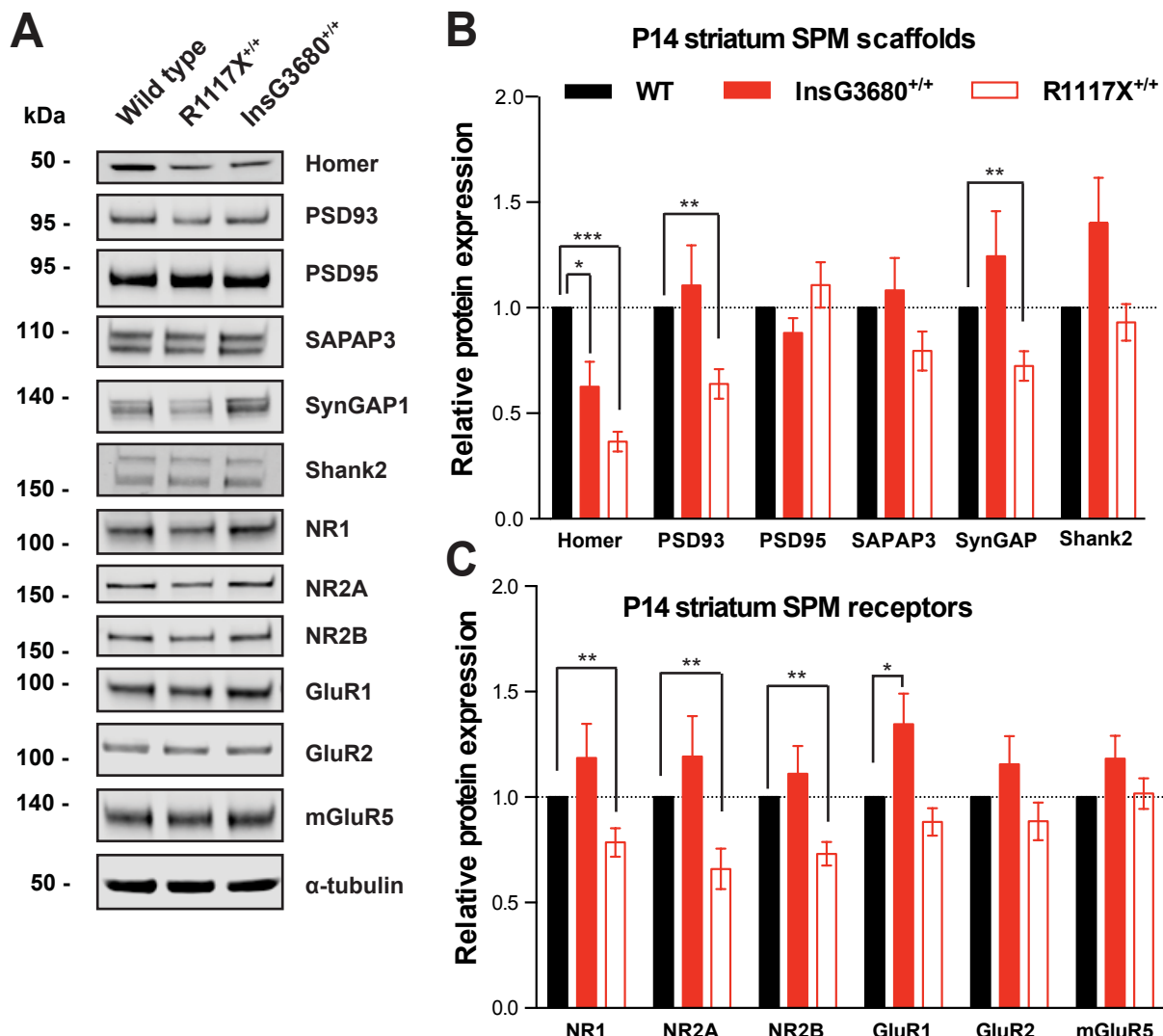


Fig S2. *R1117X^{+/}* and *InsG3680^{+/}* mice show differential abnormalities in striatal protein expression during early development (p14). Related to Figure 2.

(A) Representative blots for proteins detected by specific antibodies in the striatal SPM fraction from wild type, *InsG3680^{+/}* and *R1117X^{+/}* mice.

(B and C) Quantification of relative levels of proteins as normalized to tubulin expression from striatal SPM. (n = 8 samples per protein per genotype, each n being pooled tissue from three mice). Data are presented as mean \pm SEM. *P < 0.05, **P < 0.01, ***P < 0.001; one sample t-test.

Fig S3

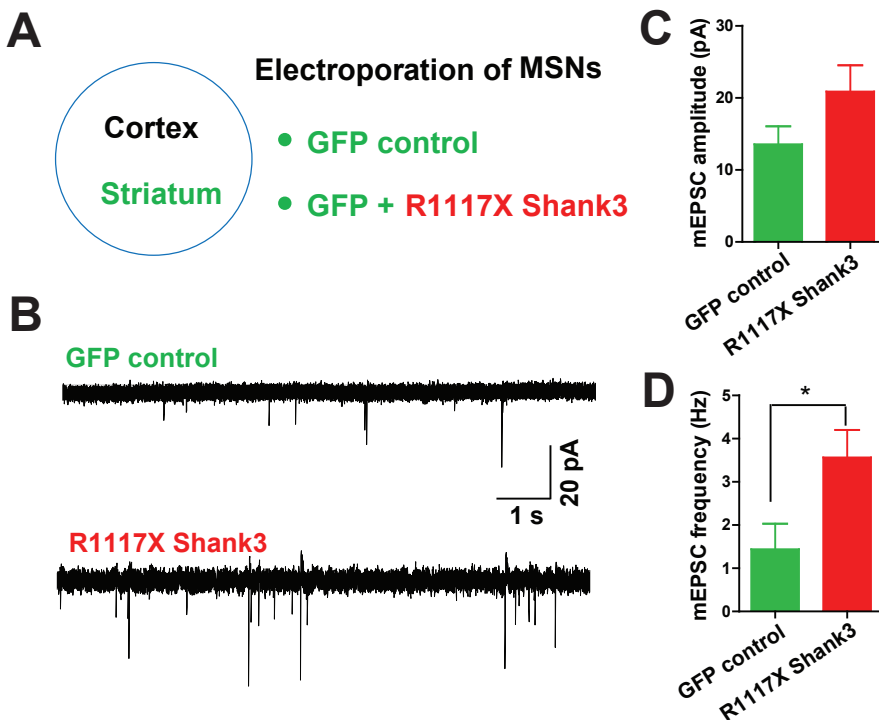


Fig S3. R1117X Shank3 increases synaptic transmission in young MSNs.

Related to Figure 2.

(A) Schematic diagram of experimental design. Striatal MSNs derived from P0 Shank3B knock mice were electroporated with either GFP plasmid or GFP plus R1117X Shanks plasmids, then plated with cortical neuron at a ratio of 3:1

(B) Representative mEPSC traces from young MSNs at DIV 8 transfected with indicated plasmids.

(C and D) R1117X Shank3 transfected MSNs tend to display increased mEPSC amplitude and significantly higher mEPSC frequency at DIV 8. Data are presented as mean \pm SEM. * $P < 0.05$; two tail t-test. n = 5 neurons per group.

Fig S4

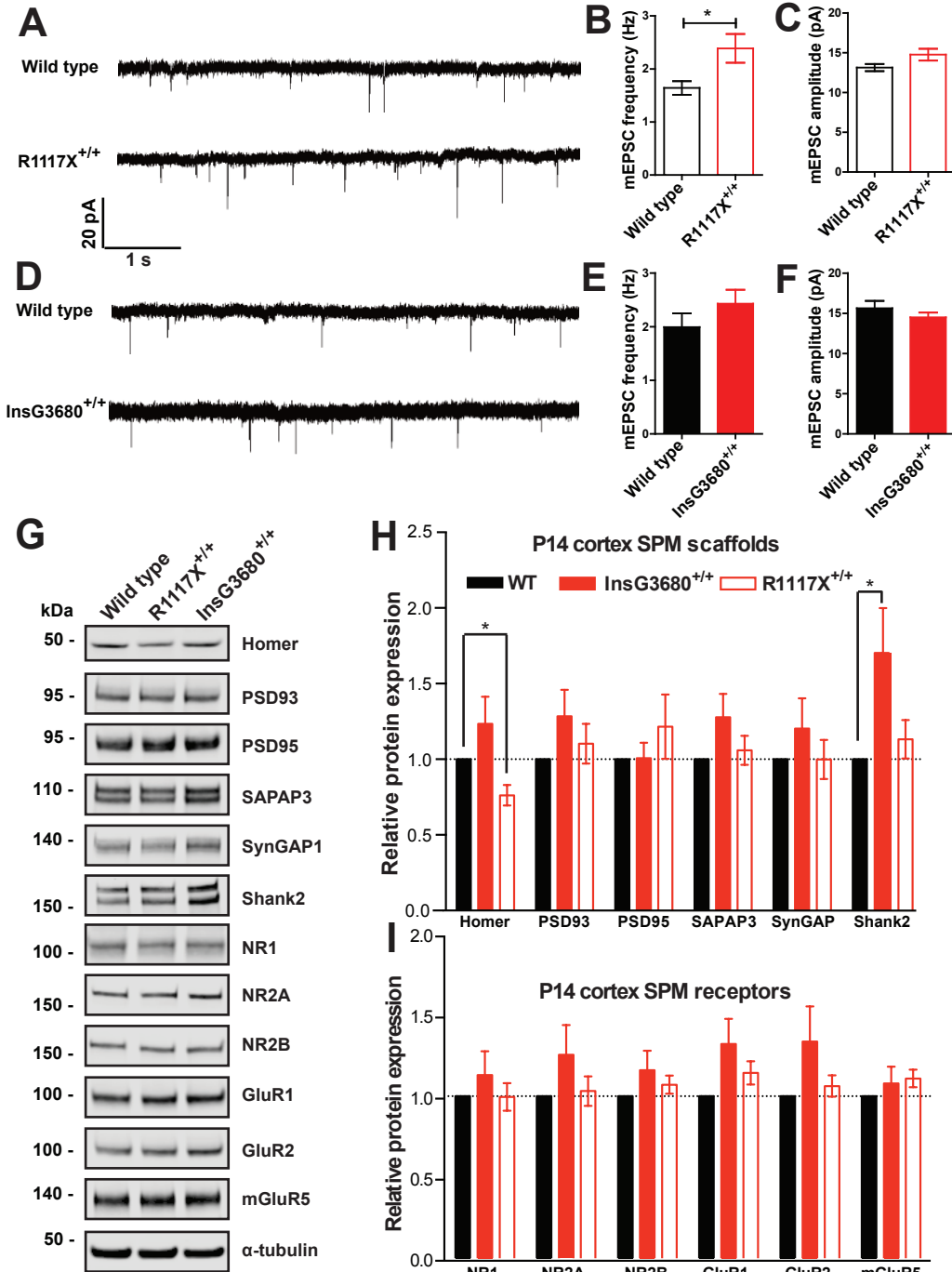


Fig S4. Electrophysiological, biochemical characterization of cortical synaptic transmission and protein expression during early development (p14). Related to Figure 2.

(A-C) mPFC neurons of R1117X^{+/+} mice display increased frequency of mEPSCs at P14. n = 21 neurons for wild type; n = 18 neurons for R1117X^{+/+} from three pairs of littermates.

(D-F) mPFC neurons of InsG3680^{+/+} mice display normal frequency and amplitude of mEPSCs at P14. n = 20 neurons for wild type; n = 19 neurons for InsG3680^{+/+} from three pairs of littermates. Data are presented as mean ± SEM. * P < 0.05; two-tailed t-test.

(G) Representative blots for proteins detected by specific antibodies in cortical SPM fraction.

(H and I) Quantification of relative levels of proteins as normalized to tubulin expression from cortical SPM. (n = 8 samples per protein per genotype, each n being pooled tissue from two mice). Data are presented as mean ± SEM. * P < 0.05; one sample t-test.

Fig S5

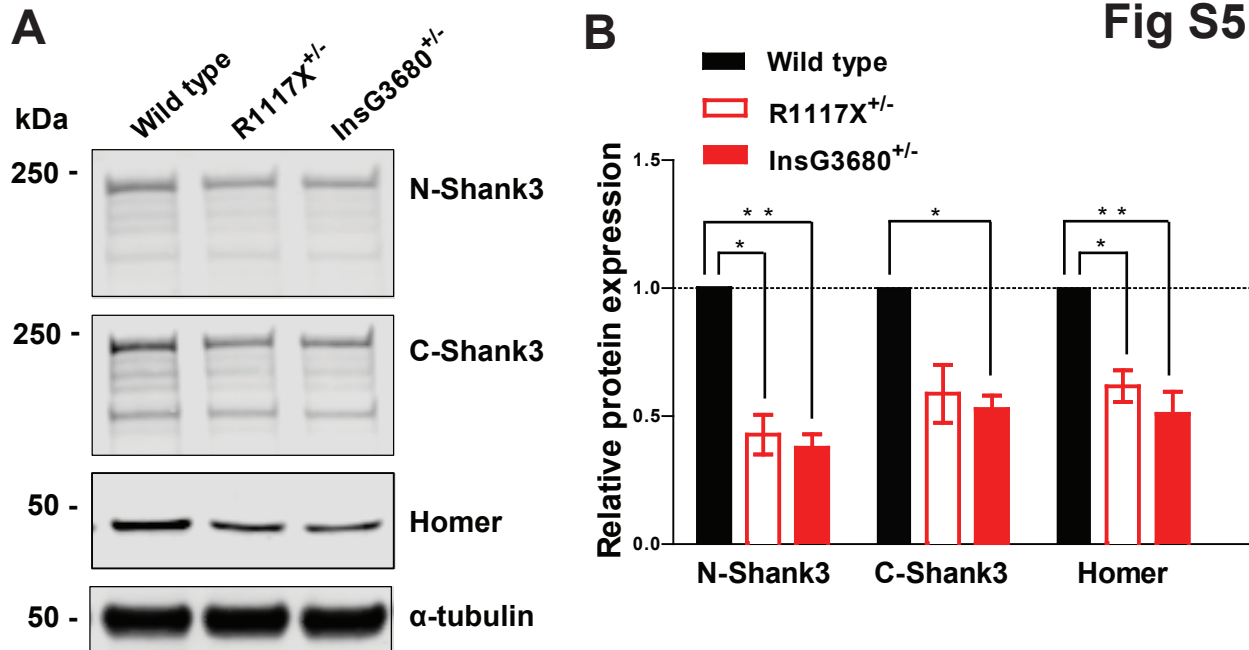


Fig S5. Reduced Shank3 and Homer protein expression in both R1117X and InsG3680 heterozygous mice. Related to Figure 6.

(A) Representative western blots using striatal SPM prepared from wild type, R1117X^{+/−} and InsG3680^{+/−} mice with indicated antibodies.

(B) Quantification of relative levels of proteins as normalized to tubulin protein expression from striatal SPM. (n = 4 samples per protein per genotype, each n being pooled tissue from three mice). Data are presented as mean ± SEM. *P < 0.05, **P < 0.01; one sample t-test.

Fig S6

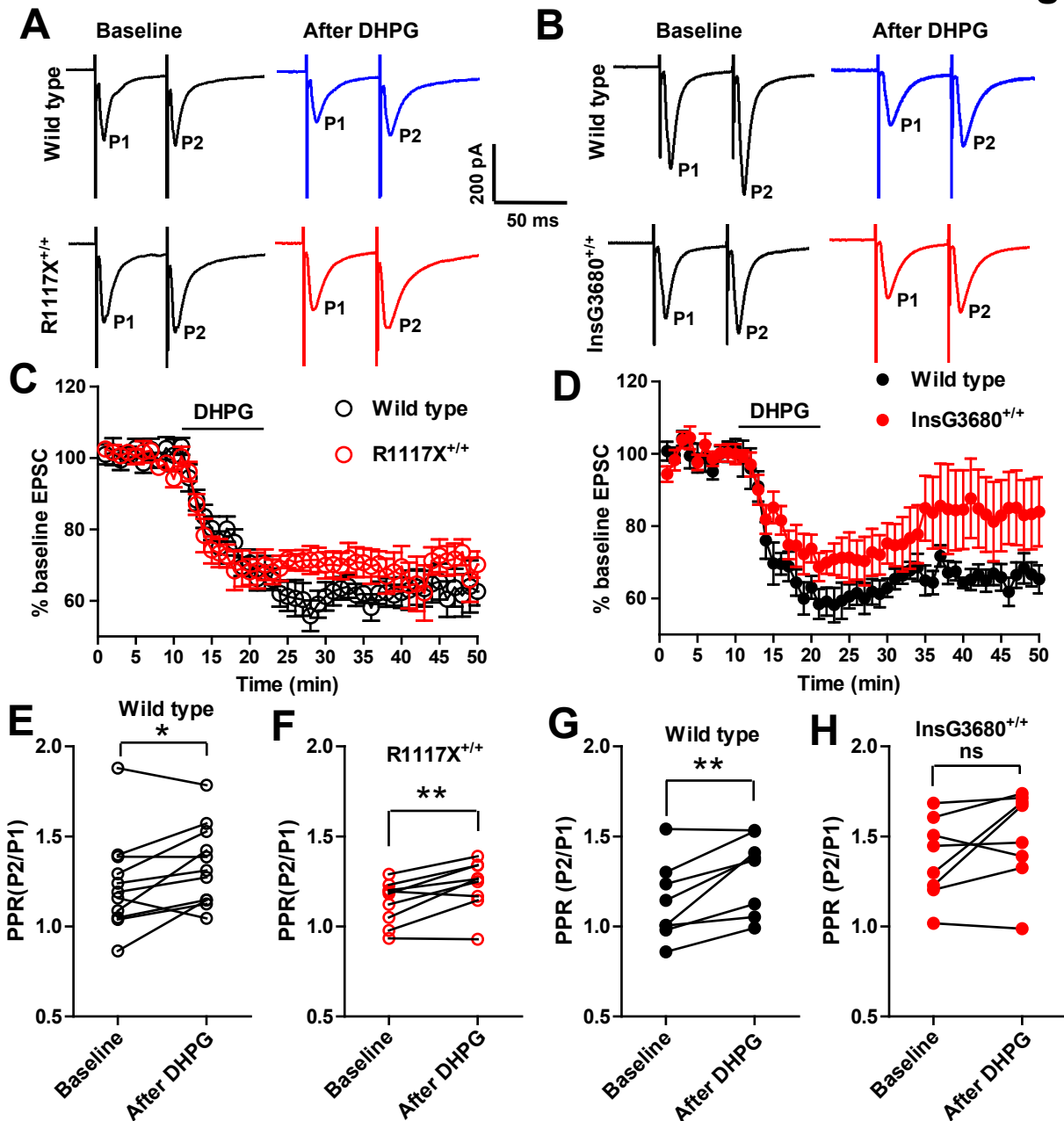


Fig S6. DHPG induced striatal LTD mediated by group I mGluRs is impaired in InsG3680^{+/+} but not R1117X^{+/+} mice. Related to Figure 6.

(A and B) Representative evoked EPSC traces (averaged amplitude of responses during the 10 min baseline and 15-25 min after DHPG perfusion) from neurons with indicated genotypes.

(C and D) Normalized amplitude of first peak (P1) of evoked EPSCs as a function of time before, during and after DHPG perfusion. In the R1117X group, n = 11 neurons for wild type, n = 9 neurons for R1117X^{+/+} from 4 pairs of mice. In the InsG3680 group, n = 8 neurons for wild type, n = 8 neurons for InsG3680^{+/+} from 4 pairs of mice.

(E-H) Increased paired pulse ratio after DHPG perfusion in wild types from both lines and R1117X^{+/+} but not InsG3680^{+/+} mice. Data are presented as mean \pm SEM, *P < 0.05, **P < 0.01; paired two-tailed t-test.

Fig S7

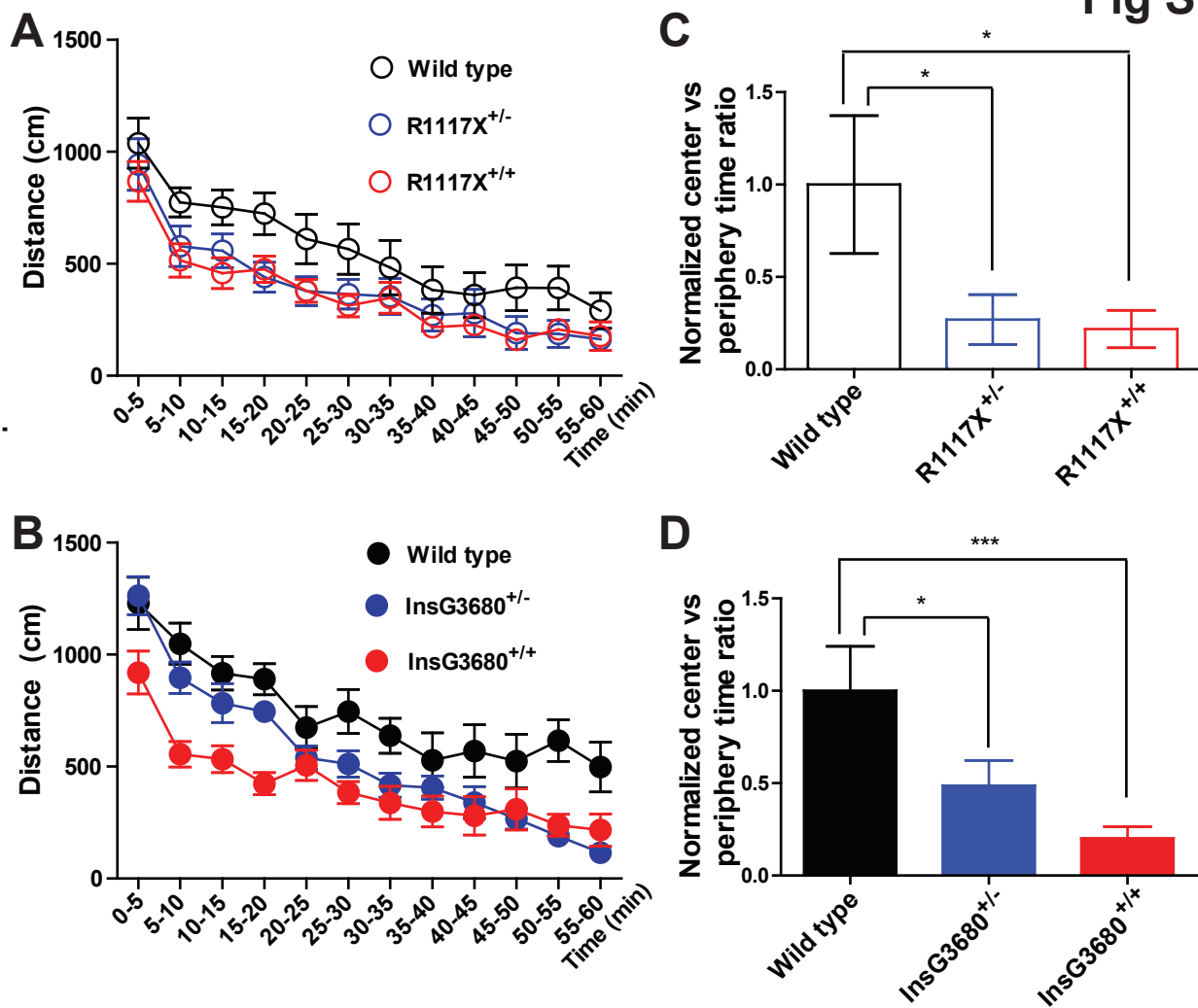


Fig S7. Normal habituation and reduced center vs periphery time ratio during open field test in both R1117X and InsG3680 Shank3 mutant mice. Related to Figure 7.
 (A and B) Distance travelled as plotted every 5 min during open field test in R1117X and InsG3680 cohorts. In the R1117X cohort, n = 15 mice for wild type; n = 15 mice for R1117X^{+/−}; n = 15 mice for R1117X⁺⁺. In the InsG3680 cohort, n = 17 mice for wild type; n = 19 mice for InsG3680^{+/−}; n = 18 mice for InsG3680⁺⁺. Data are presented as mean ± SEM. Significant differences of distance (**P < 0.001) were found from all genotypes using time as variable factor with two-way ANOVA test.
 (C and D) Center vs periphery time ratio from R1117X and InsG3680 cohorts in the open field test as normalized to their wild type littermates. Data are presented as mean ± SEM, *P < 0.05, ***P < 0.001; one-way ANOVA with Bonferroni post hoc test.

Fig S8

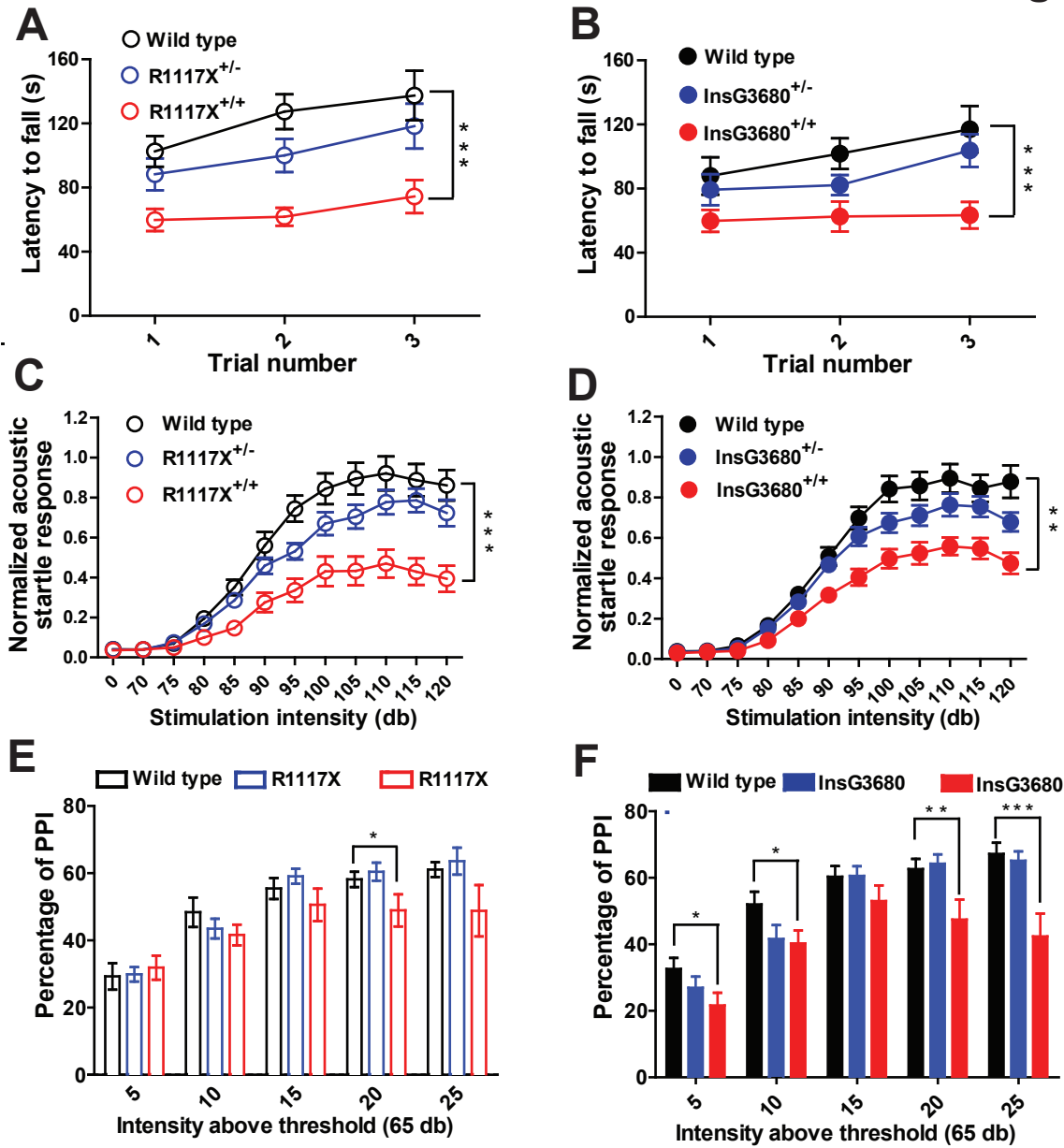


Fig S8. Impaired motor learning and startle response in both R1117X^{+/+} and InsG3680^{+/+} mice. Related to Figure 8.

(A and B) Statistical results of rotarod test from R1117X and InsG3680 cohorts. In the R1117X cohort, n = 15 mice for wild type; n = 15 mice for R1117X^{+/−}; n = 15 mice for R1117X^{+/+}. In the InsG3680 cohort, n = 16 mice for wild type; n = 19 mice for InsG3680^{+/−}; n = 18 mice for InsG3680^{+/+}. Data are presented as mean ± SEM, ***P < 0.001; two-way ANOVA with Bonferroni post hoc test.

(C and D) Impaired acoustic startle response in both R1117X^{+/+} and InsG3680^{+/+} mice.

(E and F) Impaired pre-pulse inhibition in both R1117X^{+/+} and InsG3680^{+/+} mice. In R1117X cohort, n = 16 mice for wild type; n = 18 mice for R1117X^{+/−}; n = 16 mice for R1117X^{+/+}. In InsG3680 cohort, n = 16 mice for wild type; n = 16 mice for InsG3680^{+/−}; n = 14 mice for InsG3680^{+/+}. Data are presented as mean ± SEM, *P < 0.05, **P < 0.01, ***P < 0.001; two-way ANOVA with Bonferroni post hoc test.

Supplemental table S1 (Related to Figures 1, 5, 6):

List of antibodies and their working condition

Protein	Antibody	Species	Vendor	Dilution	Blocking Buffer
SynGAP	D88G1	Rabbit mAb	CST	1 to 1000	5% BSA
GluR1	#MAB226 3	Mouse	Millipore	1 to 1000	5% milk
GluR2	32-0300	Mouse (IgG2a)	Invitrogen	1 to 500	5% milk
PSD95	ab18258	Rabbit	Abcam	1 to 1000	5% milk
Homer	AB5875	Rat	Chemicon	1 to 1000	5% milk
NR2A	07-632	Rabbit	Millipore	1 to 1000	5% milk
NR2B	N59/36	Mouse	NeuroMAB	1 to 1000	5% milk
NR1	556308	Mouse (IgG2a)	BD Pharmingen	1 to 1000	5% milk
Shank1	162 002	Rabbit	Synaptic Systems	1 to 1000	5% BSA
Shank2	#12218	Rabbit	CST	1 to 500	5% BSA
Shank3N	N367/62	Mouse (IgG2a)	NeuroMab	1 to 100	5% milk
Shank3C	SC-30193	Rabbit	Santa Cruz	1 to 1000	5% milk
SAPAP3	homemade	Rabbit	Feng lab	1 to 1000	5% milk
PSD93	ABR- 01252	Rabbit	Dianova	1 to 1000	Odyssey blocking buffer
mGluR5	ab76316	Rabbit	Abcam	1 to 5000 (unboiled sample)	5% milk

Supplemental Table S2. Molecular, biochemical, morphological, electrophysiological and behavioral phenotypes of R1117X and InsG3680 Shank3 mutant mice. Related to Figures 1-8.

		R1117X Shank3		InsG3680 Shank3	
		Heterozygous	Homozygous	Heterozygous	Homozygous
Molecular changes of Shanks	Shank3 mRNA	ND	reduced	ND	reduced
	Shank1 mRNA	ND	normal	ND	Upregulated in cortex
	Shank2 mRNA	ND	normal	ND	Upregulated in cortex
Biochemical changes of Shanks	Shank3 protein	About 50% reduced	Expression of truncated R1117X Shank3 isoform	About 50% reduced	No expression of truncated InsG3680 Shank3 isoform detected
	Shank1 protein	ND	normal	ND	Trend of increase in cortex
	Shank2 protein	ND	normal	ND	Upregulated in cortex
Biochemical changes of other synaptic proteins	Adult cortical SPM	Reduced Homer	Reduced Homer, PSD95, PSD93, SynGap, NR1	Reduced Homer	Reduced Homer, PSD95, PSD93, Trend of reduced NR1 and SynGap
	P14 cortical SPM		Reduced Homer, trend of increased GluR1		Trend of increased scaffolding proteins and receptors
	Adult striatal SPM	Reduced Homer	Reduced Homer, PSD95, SynGap, NR1, NR2B, Trend of reduced NR2B, SAPAP3 and GluR2	Reduced Homer	Reduced Homer, SAPAP3, SynGap, NR1, NR2A, NR2B, GluR2, mGluR5
	P14 striatal SPM	ND	Reduced Homer, PSD93, SynGap and NMDA receptor subunits	ND	Reduced Homer; Trend of increased scaffolding proteins and receptors; Significant increase of GluR1
Synaptic and electrophysiological phenotypes	Adult Prefrontal cortex	Reduced spine number; Reduced mEPSC frequency	Reduced spine number; Reduced mEPSC frequency and amplitude	No reduction detected	Reduced spine number
	P14 prefrontal cortex	ND	Increased mEPSC frequency	ND	Normal

	Adult dorsal lateral striatum	Reduced mEPSC amplitude	Reduced mEPSC frequency and amplitude; Reduced pop spike amplitude; Reduced NMDA current; normal DHPG induced LTD	Reduced mEPSC frequency	Reduced mEPSC frequency and amplitude; Reduced pop spike amplitude; Reduced NMDA current; impaired DHPG induced LTD
	P14 dorsal lateral striatum	ND	Normal	ND	Reduced pop spike amplitude; Increased mEPSC amplitude
Behavioral phenotypes	Pups ultrasonic vocalization	ND	Normal	ND	Normal
	Juvenile social play	ND	normal	ND	Reduced reciprocal interaction
	Anxiety related behaviors	Increased anxiety level	Increased anxiety level	Increased anxiety level	Increased anxiety level
	Locomotor activity	Reduced	Reduced	Reduced	Reduced
	Working memory tested by T maze	ND	Normal	ND	Normal
	Acoustic startle response	Normal	Impaired	Normal	Impaired
	Prepulse inhibition test	Normal	Mild impaired	Normal	Severely impaired
	Motor learning and coordination	Normal	Impaired	Normal	Impaired
	Social interaction	Impaired	Impaired	Normal	Impaired
	Repetitive behaviors	Normal	Trend of increase repetitive grooming; Low penetrance of skin lesion	Normal	Increased repetitive grooming; High penetrance of skin lesion
	Allogrooming and dominant behavior	High penetrance of allogrooming; Increased dominance-like behavior	No allogrooming behavior; Increased dominance-like behavior	Low penetrance of allogrooming; No dominance-like behavior	No allogrooming behavior; Increased dominance-like behavior

Supplemental experimental procedures

Generation and breeding of mutant mice

R1117X and InsG3680 *Shank3* mutant mice were generated by homologous recombination in R1 mouse ES cells and implanted in C57 blastocysts using standard procedures. R1117X and InsG3680 *Shank3* targeting vectors were constructed and introduced separately into R1 ES cells to replace the corresponding wild type allele. Homology arms with about 800 bp of size on both sides were designed to flank the desired point mutation, a pair of TALE nuclease plasmids were also designed as previously described (Sanjana et al., 2012) to facilitate the recombination through co-electroporation into ES cells together with targeting vector. The neo cassette was removed after targeting. High percentage chimeric mice were backcrossed with C57BL/6J (Jackson laboratory) to establish germline transmission followed by backcrossing with C57 BL/6J for five to six generations. Genotypes were determined by PCR of mouse tail DNA using the following primer pairs and gave rise to a band of 400 base pairs for wild type allele and 478 for R1117X mutation allele:

Primer F (5'-ATCTGCCATCCCTACAACCCTCC-3');

Primer R (5'-TCTCTCCGAGCAGGCAGTGGAAATCC-3')

For InsG3680, the following primer pairs were applied and generated a band of 407 base pairs for wild type allele and 486 for InsG3680 mutation:

Primer F (5'-TGCAAACCCGAGACTCTGAGAGAGGG -3');

Primer R (5'-AGCGAATACCAGCTCTGGCTCCTCC -3').

To build the colony with C57 B6/S129 Sv mixed genetic background, we crossed the F5 heterozygous mutants with S129 Sv wild type mice (Jackson laboratory) to generate the founder population, and then set up heterozygous x heterozygous brother-sister mating between these founders to generate offspring with C57B6/S129Sv mixed genetic background for all the experiments in this study. Animals were housed at a constant temperature of 23°C with a 12 h light/dark cycle with free access to food and water. Mice were housed 4–5 by genotype per cage with the exception of the animals individually housed for grooming assay.

Grooming behavior test

Adult male mice about 5 months-old were used for analysis of grooming behavior. Animals were individually housed for 2 weeks before video taping for 2 hours under red light illumination between 7:00-9:00 pm. Grooming behaviors were manually coded and analyzed using Noldus Observer software, so that the total duration that an animal spent on grooming in the 2 hours segment was determined and normalized to its mobile time. Grooming included all sequences of face-wiping, scratching/rubbing of head and ears, and full-body grooming.

Open field test

Spontaneous locomotor activity was assessed as total distance travelled (m) over 60 min in an automated Omnitech Digiscan apparatus (AccuScan Instruments) as described previously (Peca et al., 2011). Activity was quantified over a 60 minute period by a computer operated detecting system.

Elevated zero maze test

The elevated zero maze consists of a circular platform that is equally divided into four quadrants. The zero maze was indirectly illuminated at 60 lux on the open arms and 10 lux on the closed arms. Testing started with an animal being placed into a closed arm of the maze. Behavior was video-taped for 5 min and then scored by a trained observer using Noldus Observer software. Anxiety-like behavior was interpreted based upon the percentage of time that mice spent in the open arms. The animals used in the elevated zero maze test were previously tested in the open field assay with one-week's break.

Three-chamber social interaction test

Sociability and social novelty test were performed as previously described (Chao et al., 2010; Peca et al., 2011) with minor modifications. Briefly, 3 months-old male mice were used across all cohorts. Both stranger 1 and stranger 2 were wild type male S129 Sv males (Jackson laboratory) with matched age and body weight to test mice. Stranger mice were habituated by placing them inside an inverted wire cup for 30 min, two sessions per day for three consecutive days before experiments. Each stranger mouse was used maximally two times per day. Test mice were habituated to the facility environment for 1 hour before the start of behavioral tasks. The social test apparatus was made of a clear plexiglass box (65 (L) × 44 (W) × 30 (H) cm) with removable floor and partitions dividing the box into left, center, and right chambers. Center chamber (21 cm x 22 cm) is half the width of left (21 cm x 44 cm) and right chamber (21 cm x 44 cm). These three chambers were interconnected with 5 cm openings between each chamber which can be closed or opened manually with a lever operated door. The inverted wire cups to contain the stranger mice were cylindrical, 10 cm in height, a bottom diameter of 10 cm with the metal bars spaced 0.8 cm apart. A weighted cup was placed on top of the inverted wire cups to prevent the test mice from climbing onto the wire cup. Each wire cup was used only one time per day then followed by extensive clean with 75% ethanol and water at the end of the test day. During the habituation phase, an empty wire cup was placed into left and right chamber, and the test mouse was placed into the middle chamber and allowed to explore for 15 minutes, with the doors into both side chambers open. During the sociability test phase, the test mouse was firstly gently introduced to the middle chamber with the doors to both side chambers closed, and an unfamiliar mouse (S1) was placed under the inverted wire cup in one of the side-chambers and a toy object (O) was placed under the inverted wire cup placed on the opposite side chamber. The location of the stranger mouse and object was counterbalanced between test trials to exclude side preference. The experimenter then lifted up the doorways to both side chambers simultaneously, and the test mouse was allowed to explore all three chambers for 15 minutes. During the social novelty test phase, the test mouse was again gently introduced into the middle chamber with the doors to both side chambers closed. Then a novel mouse (S2) was placed under the inverted wire cup, replacing the toy object (O) in one of the side-chambers. The experimenter then lifted up the doorways to both side chambers simultaneously, and the test mouse was allowed to explore all three chambers for an additional 15 minutes. Time spent in close proximity to the stranger mice or toy object was analyzed using the

Noldus Ethovision software. The animals used in the social interaction test were previously tested in the zero maze assay with one-week's break.

Tube test

The tube test assay was performed as previously described (Wang et al., 2011a). We used transparent plexiglass tubes with 30 cm length and 3 cm inner diameter. This narrow space is just sufficient for an adult mouse (4-5 month-old) to walk through without being able to reverse its body direction. Mice were habituated to walk through the tube two sessions per day for four consecutive days before testing. On the day of testing, two unfamiliar mice with different genotypes were pushed to the middle of the tube and released simultaneously. The mouse that completely retreated first from the tube within the first 6 min of the test was defined as the loser, and the other as the winner. In very rare cases, when no mice retreated within 6 min, the tests were repeated. The same pair of mice was matched again on the same test day with mice entry sides counterbalanced. The tubes were cleaned with 75% ethanol between trials. A chi-square analysis was applied to determine the significance of test score between mice when compared with an outcome expected by chance (i.e. a 50:50 win–lose outcome).

Juvenile play behavior

Juvenile play behavior test was performed as described previously (Penagarikano et al., 2011). The juvenile play apparatus was made of a non-transparent plexiglass box (32 (L) × 32 (W) × 32 (H) cm) and indirectly illuminated with 10 lux inside. Test mice were weaned at P21 and individually habituated inside the test chamber with a thin layer of bedding for two consecutive days, with two sessions per day and half an hour per session. Test mouse at P23 was gently placed into the test chamber with an unfamiliar mouse matched in genotype, gender and age. This pair of test mice was then video-taped for 10 min. The time that mice engaged in typical social interaction behaviors, including nose-to-nose sniff, nose-to-anogenital sniff, following/chasing behavior, were scored using EthoVision XT 9 (Noldus) by trained observers blinded to genotypes.

Ultrasonic vocalization test

Ultrasonic vocalization test was performed as described previously (Schmeisser et al., 2012). A sensitive microphone was placed 20 cm above the center of the recording cage, which was with fresh clean bedding and located in a sound-attenuating chamber to block background noise. The microphone was connected to an ultrasound recording device, UltraSoundGate 116H (Avisoft Bioacoustics), connected to a personal computer installed with the recording software Avisoft Recorder (Avisoft Bioacoustics). The recording parameters were: sampling frequency 250 kHz with 16-bit format. Pups from multiple cohorts were individually separated from their mother and littermates, and were placed in the recording chamber, where their USVs were recorded for 10 min. Recordings were performed on every second day between postnatal days P2-P12. The home cage with the pups and mother, as well as the recording cage itself, were placed on a heating pad set at 32 °C to prevent any temperature-related stress that will affect the USVs. USV recordings were analyzed using Avisoft SASLabPro (Avisoft Bioacoustics), conducting a fast Fourier

transform (512 FFT length, 100% frame, Hamming window with 75% time window overlap, amplitude threshold -55dB, hold-time 10ms).

Acoustic startle response and prepulse inhibition test

Acoustic startle response and prepulse inhibition tests were performed as previously described (Gould et al., 2005; Joober et al., 2002). Mice were tested between 4~5 months of age and maintained on a 12 hours light/dark cycle (lights on at 07:00 am) with free access to food and water. Experiments were performed between 9 am and 4 pm with two identical sound attenuating test chambers (65 cm×35 cm×25 cm). Each test chamber was equipped with a loudspeaker mounted 25 cm above the holding cylinder and a commercial startle reflex system (SR Lab, San Diego Instruments, CA). Individual mouse was placed inside the plexiglass holding cylinder mounted on a plexiglass platform. A piezoelectric accelerometer located beneath the platform was used to transform startle responses into units based on force and latency of startle. Data were collected at 250 samples/s and the maximum voltage attained on each trial was used as the dependent variable. Each test session started with a 5 min acclimation period in the presence of 65 dB acoustic background noise followed by five 120 dB startle pulses. Pre-pulse trials followed the initial 120 dB startle acclimation. Each pre-pulse stimulation was 20 ms in duration, followed by a 40 ms startle stimulus of 120 dB. PPI was recorded for pre-pulse intensities of 70, 75, 80, 85 and 90 dB, and no stimulus. Each prepulse trial was administered ten times in a random order. Trials of 120 dB alone were randomly interspersed within the pre-pulse trials and used for comparison with the prepulse trials. The percent PPI was calculated using the formula [100–(response to pre-pulse + 120 dB)/(response for 120 dB alone)×100]. Acoustic startle trials were followed the PPI trials. Startle trials consisted of 40 ms pulses at 0 (no stimulus), 70, 75, 80, 85, 90, 95, 100, 105, 110, 115, and 120 dB. Each trial was presented five times in a randomized order.

T maze spontaneous alternation

T maze spontaneous alternation test was performed as described previously (Deacon and Rawlins, 2006). Briefly, adult mice of 5~6 months old were accustomed to handling by the experimenter for ten minutes for two consecutive days. A thin layer of bedding was placed on the floor of the T maze and changed freshly between mice. The mouse was gently introduced into the start box of the T maze and was allowed to freely explore either left or right arm of the maze for nine or ten consecutive trials. A choice was determined to be made when the test mice stepped into one arm with all four paws. At that moment, the gate of the opposite arm was closed and the animal was allowed to explore the chosen arm for 10 s and return to the start box before the next trial. Between trials, the mouse was confined for 30 s in the start box, and the gate of the unexplored arm was removed. Trials were run for three consecutive days.

Rotarod test

Motor coordination was assessed as previously described (Peca et al., 2011) with an accelerating rotarod assay (4 to 40 r/m). Briefly, animals of 4~5 months age were introduced onto the apparatus

(Med Associates) and the latency to fall was determined. Animals were tested for three trials in a single day with an inter-trial interval of 30 min.

Slice preparation for adult mice

Acute brain slices were prepared from 8-weeks-old mice as described previously (Peca et al., 2011). Slices were prepared from a group of mice consisting of one wild type, one heterozygous and one homozygous with the same solution and procedure each day. Mice were deeply anesthetized by intra-peritoneal injection of avertin solution (20 mg/ml, 0.5 mg/g body weight) and then transcardially perfused with 25 ml of carbogenated (95% O₂, 5%CO₂) ice cold cutting artificial cerebrospinal fluid (aCSF) with the composition (in mM): 105 NMDG, 105 HCl, 2.5 KCl, 1.2 NaH₂PO₄, 26 NaHCO₃, 25 Glucose, 10 MgSO₄, 0.5 CaCl₂, 1 L-Ascorbic Acid, 3 Sodium Pyruvate, 2 Thiourea (pH 7.4, with osmolarity of 300–310 mOsm). The brains were rapidly removed and placed in ice-cold and oxygenated cutting solution. Coronal slices (300 µm) were sliced using Leica VT1200S (Leica Microsystems) and then transferred to a recovery chamber at 32 °C with carbogenated cutting aCSF solution for 12 min, followed by transferring to a holding chamber containing aCSF that contained (mM): 119 NaCl, 2.3 KCl, 1.0 NaH₂PO₄, 26 NaHCO₃, 11 Glucose, 1.3 MgSO₄, 2.5 CaCl₂ (pH was adjusted to 7.4 with HCl, with osmolarity of 300–310 mOsm) at room temperature. Slices were allowed to recover for one more hour in a holding chamber before recording and used for the experiment typically 2~6 hours after slicing.

Slice preparation for juvenile mice

Acute brain slices from juvenile mice were prepared as described previously (Peca et al., 2011). Briefly, a pair of wild type and homozygous mice from the same litter at postnatal day 14 were deeply anesthetized and rapidly decapitated. Dissected brain were placed into carbogenated (95% O₂, 5%CO₂) ice cold cutting artificial cerebrospinal fluid (aCSF) with the composition (in mM) 194 sucrose, 30 NaCl, 4.5 KCl, 1.2 NaH₂PO₄, 26 NaHCO₃, 10 glucose, 0.2 CaCl₂, 8 MgSO₄ (pH 7.4, 350 mOsm). Coronal slices (300 µm) were sliced in the same cutting aCSF using Leica VT1200S (Leica Microsystems) and then transferred into a recovery chamber containing carbogenated normal aCSF of the composition (in mM): 119 NaCl, 2.3 KCl, 1 NaH₂PO₄, 26 NaHCO₃, 11 glucose, 2.5 CaCl₂, 1.3 MgSO₄ (pH 7.3, 300–310 mOsm) for 15 min at 32 °C before moving to a holding chamber at room temperature. Slices were allowed to recover for one more hour in a holding chamber before recording and used for recording typically 2~6 hours after preparation.

Cortico-striatal extracellular field recording

Recording of population spikes in dorsal later striatum was performed as described (Peca et al., 2011; Welch et al., 2007). Slices were placed into recording chamber (Warner Instruments) and constantly perfused with oxygenated aCSF at room temperature at a speed of 2.0 ml/min. A platinum iridium concentric bipolar electrode (FHC) was positioned on the inner border of the corpus callosum between the cortex and dorsolateral striatum to stimulate the predominant cortical input to dorsolateral striatal region. A borosilicate glass recording electrode filled with 2M NaCl was placed onto the dorsolateral striatal region approximately 400 µm away from the stimulating

electrode. Cortico-striatal field population spikes were elicited by delivery step depolarization (0.15 ms duration with 0.5 mA intensity at a frequency of 0.1 Hz). Stable baseline response of pop spike for at least of 5 min from individual slice was ensured before moving to input-output assay. Input-output curves were determined for both the negative peak 1 (NP1; presynaptic fiber volley) and pop spike amplitude by delivery of three consecutive stimulations from 0 to 1 mA with 0.1 mA increments. Recordings were performed at room temperature and data were sampled using pCLAMP 10 software (Molecular Devices).

Whole cell patch clamp recording

Slices were placed into a recording chamber (Warner Instruments) and constantly perfused with oxygenated aCSF at room temperature at a speed of 2.0 ml/min. MSNs were visually identified with a microscope equipped with IR-DIC optics (BX-51WI, Olympus) by location, shape and other electrophysiological parameters. Recording pipettes with resistance about 3~4 M Ω were pulled with pipette puller (P-97, Sutter Instruments) using capillary glass (King Precision Glass, type 8250). Pipettes were filled with internal solution containing (in mM): 107 CsMeSO₃, 10 CsCl, 3.7 NaCl, 5 TEA-Cl, 20 HEPES, 0.2 EGTA, 5 lidocaine N-ethyl chloride, 4 ATP magnesium salt, and 0.3 GTP sodium salt (pH 7.3, osmolarity 300~305 mOsm). Series resistance between 10 to 15 M Ω was constantly monitored. Multiclamp 700B amplifier (Molecular Devices) and digidata 1440A were used to acquire whole cell signals. Signals were sampled at 10 kHz and filtered at 2 kHz. AMPA receptor-mediated mEPSCs were collected at least 5 min after forming a stable whole cell patch clamping, recordings were performed by holding the MSN at -70 mV and perfused with aCSF supplied with 50 μ M DL- APV (Abcam), picrotoxin (100 μ M) (Tocris) and 1 μ M TTX (Tocris). The mEPSCs data were analyzed with Mini Analysis program (Synaptosoft). Recording of AMPAR to NMDAR current ratio was performed and data were analyzed as described previously (Saal et al., 2003). A platinum iridium concentric electrode (FHC) was positioned on the inner border of corpus callosum between cortex and dorsolateral striatum to stimulate the predominant cortical input to dorsolateral striatal region. Recording of AMPAR and NMDAR current was conducted in the presence of picrotoxin (100 μ M) and glycine (10 μ M). Each evoked response was repeated for 15 times with an inter-stimulus interval of 20 s for all MSNs recorded. MSNs were firstly clamped at -70 mV for 5~10 min to ensure stable response of EPSC, followed by switching the holding potential to +40 mV for an additional 15~20 min to obtain AMPAR and NMDAR component of EPSC. Mixed EPSC component from both AMPAR and NMDAR was firstly recorded by averaging 15 consecutive responses before application of D-APV. Pure AMPAR mediated EPSC was collected by averaging 15 consecutive response 5 min after application of D-APV (50 μ M). Averaged NMDAR mediated EPSC was obtained by digitally subtracting the AMPAR EPSC from mixed component in the absence of D-APV. AMPAR to NMDAR current ratio is calculated by dividing the peak of AMPAR EPSC with peak of NMDAR EPSC. Series resistance was monitored online to ensure less than 15% change throughout each experiment.

Co-culture of cortical neuron and striatal MSNs

Primary corticostriatal co-cultures were prepared as described previously (Segal et al., 2003; Tian et al., 2010). Striatal tissue were prepared from newborn Shank3B knockout mouse. Cortical tissues were dissected from newborn wild type pups. Tissues were digested with papain (Worthington Biochemical Corporation) and dissociated with small glass Pasteur pipette. Before plating, about 5 million of striatal MSN were electroporated with Nucleofector™ Kits for mouse neurons (Lonza) with either 1 µg of GFP plasmid alone or 1 µg of GFP plasmid + 2 µg of R1117X Shank3 mutant plasmid. The striatal MSNs and cortical neurons were then mixed at a ratio of 3:1 and plated onto 12 mm coverslips pre-coated with Poly D-lysine/Laminin (Corning™ BioCoat™) at a density of $1 \times 10^5/\text{cm}^2$ inside a 24-well plates with Neurobasal A medium (Invitrogen) supplemented with 0.5 mM glutamine (Invitrogen), 1×B27 (Invitrogen), 50 mg/L penicillin/streptomycin (Invitrogen), 50 ng/mL BDNF (R&D Systems) and 30 ng/mL GDNF (R&D Systems). After initial plating, one fourth of the medium was exchanged with fresh medium without BDNF and GDNF every 3-4 days. GFP positive MSN neurons from either GFP control group or R1117X Shank3 transfected group were recorded on DIV8 after plating with standard electrophysiological procedure.

Evoked recording of NMDA receptor mediated EPSC

Recording of evoked synaptic current mediated by NMDA receptors was performed as previously described (Logan et al., 2007; Tsien et al., 1996). Coronal slices were placed into a recording chamber (Warner Instruments) and constantly perfused with oxygenated aCSF at room temperature at a speed of 2.0 ml/min. A platinum iridium concentric bipolar electrode (FHC) was positioned on the inner border of the corpus callosum between the cortex and dorsolateral striatum to stimulate the predominant cortical input to dorsolateral striatal region. Whole cell recording was performed on MSN at dorsolateral striatal region approximately 250~350 µm away from the stimulating electrode. Before starting the NMDA current measurement, position of stimulation electrode was moved gently to ensure the reliable evoking of at least 150 pA of AMPA receptor mediated current in the presence of 100 µM PTX when holding the MSNs at -70 mV with fixed stimulation intensity at 0.2 mA for all the MSNs . Then cocktail aCSF with drugs containing (100 µM PTX, 10 µM NBQX, 10 µM Glycine) was perfused to block all AMPA receptor mediated current. NMDAR-mediated EPSCs were evoked by a series of stimuli with intensities ranging from 0 to 1.0 mA with 0.1 mA increments when holding the MSNs at +40 mV in the presence of cocktail drugs. Each evoked response was repeated for 4 times with an inter-stimulus interval of 30 s for all MSNs recorded.

DHPG induced LTD in striatal MSNs

Recording of long term depression (LTD) from MSNs in dorsolateral striatum was performed as described previously (Yin et al., 2006). Briefly, coronal slices containing typical dorsolateral striatum were placed into a recording chamber (Warner Instruments) and constantly perfused with oxygenated aCSF in the presence of 100 µM PTX throughout all the experiments. ACSF solution was maintained between 30 °C to 31 °C at a speed of 2.0 ml/min during the experiment. A platinum iridium concentric bipolar electrode (FHC) was positioned on the inner border of the corpus

callosum between the cortex and dorsolateral striatum to stimulate the predominant cortical input to dorsolateral striatal region. Whole cell recording was performed on MSNs at dorsolateral striatal region approximately 250~350 μ m away from the stimulating electrode. Recording pipettes with typical series resistance about 3~4 M Ω were pulled with pipette puller (P-97, Sutter Instruments) using capillary glass (King Precision Glass, type 8250). Pipettes were filled with internal solution containing (in mM): 107 CsMeSO₃, 10 CsCl, 3.7 NaCl, 5 TEA-Cl, 20 HEPES, 0.2 EGTA, 5 lidocaine N-ethyl chloride, 4 ATP magnesium salt, and 0.3 GTP sodium salt (pH 7.3, osmolarity 300~305 mOsm). MSNs were voltage clamped at -50 mV during the recording (to activation the L-type calcium channels), stimulus intensity was adjusted to a level at which EPSC amplitude was between 200~400 pA. A paired pulse stimulation paradigm with 50 ms inter-stimulus interval was applied throughout the recording to confirm the successful induction of mGluRs (group I)-dependent and presynaptic mediated LTD. Paired pulse ratio (PPR) was analyzed by calculating the ratio of the amplitude of the second peak of EPSC (P2) to first peak (P1). Successful induction of LTD in MSNs was featured by reduced amplitude of EPSCs accompanied with increased PPR 15~25 min after DHPG perfusion as compared to the baseline response. We analyzed only recordings from MSNs with series resistance less than 20 M Ω . The series resistance, typically ranging from 10 to 15 M Ω , was not compensated during the recording. Any MSNs with more than 20% of changing of series resistance were excluded for data analysis. MSNs with a stable baseline response for at least 10 min were perfused with 100 μ M (RS)-3, 5-dihydroxyphenylglycine (DHPG) for 12 min, then switched to ACSF for 30 more min.

SPM and PSD preparation from mouse brain

Striatal and cortical tissue was obtained from two months old mice, experiments were performed as described previously (Peca et al., 2011). Briefly, mice were decapitated after an isoflurane overdose and the head was shock-frozen in liquid nitrogen for four seconds. Cortical (bregma 1.4 to -0.46 mm) and striatal (bregma 1.4 to -0.46 mm) regions were micro-dissected and snap-frozen on dry ice. Tissue from two mice for cortex samples or three mice for striatum samples was pooled to generate one sample (one n, approximately 200 mg brain tissue total). All the buffers and solutions used for the SPM and PSD preparation were supplied with protease inhibitor (PI, cComplete protease inhibitors from Roche). The pooled tissue was homogenized in 3 ml ice-cold buffer (4 mM HEPES pH 7.4, 0.32 M sucrose) using a 5 ml, tissue grinder (Wheaton# 358005) and power homogenizer at 900 rpm for 30-40 strokes. Homogenates were centrifuged for 15 min at 900 g at 4 °C. Supernatants were centrifuged again for 15 min at 900 g at 4 °C. Next, supernatants were centrifuged for 15 min at 18,000 g at 4 °C to obtain the crude synaptosomal fraction. This pellet was washed with 3 ml ice-cold buffer (4 mM HEPES pH 7.4, 0.32 M sucrose with PI) and centrifuged for 15 min at 18,000 g at 4 °C. The washed pellet was dissolved in 3 ml hypo-osmotic buffer (4 mM HEPES pH 7.4). Using the tissue grinder, 8 strokes were manually applied. Then the hypo-osmotic synaptosomal fraction was rotated for 1 h at 4 °C. Hypo-osmotic synaptosomal fractions were centrifuged for 20 min at 26,500 g at 4 °C and the pellets were snap frozen on dry ice. The pellets were supplemented with 300-400 μ l buffer (50 mM HEPES pH 7.4, 2 mM EDTA) and dissolved via sonication (4°C, 10 % power, 30 % ON, 70 % OFF, 30 s, Omni-

Ruptor 250). Using the bicinchoninic acid protein assay (Thermo Scientific Pierce), protein concentrations were measured for each sample. To prepare the PSD fraction, pellets of synaptosomal fractions were dissolved in 0.1 ml ice-cold buffer (4 mM HEPES pH 7.4, 0.32 M sucrose) and placed on top of the sucrose gradient 0.8 M/1.0 M/1.2 M (27%, 34%, 41%) in a Beckman ultracentrifuge tube (347356) with 500 μ l/layer. Purification was performed by ultracentrifugation using swing bucket rotor TLS-55 at 117,257 g (42,000 rpm) for 2 hours at 4 °C. Enriched PSD fraction was harvested using a 1 ml insulin-syringe with needle to punch a hole on the side around the interface between layer of 1.0 M and 1.2 M. About 400-600 μ l of fraction was extracted and diluted to 0.32 M sucrose by adding 2.5x volume of HEPES buffer. Dissolved pellets were further spinned at 128,405 g for 30 min (55,000 rpm in TLA100.3). Pellet was resuspended after centrifuge with 1 ml of HEPES buffer (50 mM HEPES pH 7.4, 2 mM EDTA) followed by adding Triton X-100 to 0.5% (52.6 μ l Triton X-100 10%). Sample was mixed thoroughly and rotated at 4 °C for 15 min then spun at 32,000g for 20 min (28,000rpm with TLA-100.3 rotor). Next 1 ml ice-cold HEPES-C/ea was added to the pellet (PSD-1T), then 0.5% Triton X-100 (52.6 μ l Triton X-100 10%). Sample was mix thoroughly and rotated at 4 °C for 15 min. Centrifugation was again performed at 200,000g (65,000 rpm TLA-100.3) for 20 min to obtain PSD-2T pellet. Following recovery of the PSD-2T pellet in 100 μ l of HEPES buffer (50 mM HEPES pH 7.4, 2 mM EDTA), 14.24 μ l 20% SDS and 43.94 μ l 9M Urea was added. Brief sonication with 10% power and 3 pulses (30% ON-70% OFF) was used to dissolve the pellets. Lastly, aliquot PSD fraction was aliquoted and stored at -80 °C before protein quantification and western blotting assays.

Western blotting and quantification

The dissolved samples were mixed with 400 μ l 2x Laemmli sample buffer (Bio-Rad). 400 μ l of the mixture was kept without boiling and 400 μ l was boiled for 5 min at 95 °C. Sample volumes corresponding to 25 μ g protein per lane were loaded onto 4-15 % gradient Mini-PROTEAN TGX gels (Bio-Rad) and run for 3 h at 50 V. The proteins were then transferred onto Whatman Protran nitrocellulose membranes (0.2 μ m pore size, BA83, Sigma-Aldrich) using a tank blot system (Mini Trans-Blot Cell, Bio-Rad) for 120 min at 100 V at 4 °C. The membranes were blocked for 1 h with the respective blocking buffer (supplementary table 1) that did not contain any Tween-20. Subsequently, the membranes were incubated with primary antibodies diluted in blocking buffer (supplementary table 1) for 12 hrs at 4 °C. Following primary antibody incubation, the membranes were washed three times for 5 min per wash using TBST buffer (0.05 % Tween-20). Then, the secondary antibodies, goat-anti-mouse IRDye680 (Li-COR Biosciences), donkey-anti-rabbit IRDye 800CW (Li-COR Biosciences) or goat-anti-rat IRDye 800CW (Li-COR Biosciences), diluted in 1:1 TBST (0.05 % Tween-20): Odyssey Blocking Buffer (Li-COR Biosciences) were incubated with the membrane for 2 hrs at room temperature. Following three rounds of washing with TBST, the membranes were scanned using an Odyssey CLx infrared imaging system (Li-COR Biosciences). Specific bands were then quantified with the contrast-independent, automatic background subtraction rectangular ROI tool of the built-in Software Image Studio 3.1 (Li-COR Biosciences) and normalized to an alpha-tubulin loading control for each lane and each blot. The

values obtained for the mutation genotypes were then normalized to the wild-type expression. Statistical significance was tested for using the one-sample t-test for normalized values by asking whether the measured value differs significantly from the hypothetical value 1.0 (wild-type levels).

Golgi staining and spine counting

Golgi staining and spine counting was performed as described previously (Schmeisser et al., 2012). Three littermate pairs of male mice at two-months old from both R1117X and InsG3680 cohort were used for spine counting. Golgi staining of mouse brain was carried out according to the standard user manual (FD Rapid GolgiStain™ Kit). Briefly, dissected adult mouse brains were firstly immersed into impregnation solution (solution A+B) for 14 days in the dark, followed by incubating in solution C for 3 day before slicing. To prepare slices for imaging, coronal slices were prepared at 100 µm thickness using vibratome. Z-stack confocal images were taken using an Olympus FluoView 1000 laser scanning confocal microscope. To quantify the spine density, images of at least ten neurons at the layer II/III of frontal association area for each mouse brain were taken with only one branch per neuron. Slices were imaged and the density of spines were counted by an experimenter blind to the genotype of the mice.

RNA isolation and Q-PCR assay

Tissue was obtained from age-and gender-matched brains of wild type, R1117X^{+/+} and InsG3680^{+/+} mice. Briefly, adult mice were decapitated after an isofluorane overdose and the head was shock-frozen in liquid nitrogen for four seconds. Cortical (bregma 1.4 to -0.46 mm) and striatal (bregma 1.4 to -0.46 mm) regions were micro-dissected and snap-frozen on dry ice. Quantitative PCR was performed as described previously (Wang et al., 2014). Total RNA was extracted using the RNeasy mini kit (QIAGEN) following the standard user manual. Equivalent amount of total mRNAs were reversely transcribed to cDNAs with iScript cDNA Synthesis Kit (Bio-Rad). Quantitative real-time PCR (q-PCR) was carried out using the iQ5 real-time PCR detection system (Bio-Rad) with the iQ SYBR Green Super mix kit (Bio-Rad) following the guidance of manufacturer's manual. The primers used in this study are listed below:

Shank3 Exon 1 RT forward: 5'-CCGGACCTGCAACAAACGA-3'
Shank3 Exon 2 RT reverse: 5'-GCGCGTCTTGAAGGCTATGAT-3'
Shank3 Exon 6 RT forward: 5'-GTTGCGAGCTGCTTCTCCAT-3'
Shank3 Exon 8 RT reverse: 5'-GCGCAACTCTCCTGGTTGTA-3'
Shank3 Exon 16 RT forward: 5'-GGTTGGACACAAGCAAGTGG-3'
Shank3 Exon 17 RT reverse: 5'-CAGCCGTCATGGACTTGGAC-3'
Shank3 Exon 21 RT forward: 5'-CGGAAGCTTGACGAGAAC-3'
Shank3 Exon 21 RT reverse: 5'-CTCATCAATGGAGCGGGAGG-3'
Shank1 RT forward: 5'-CCGCTACAAGACCCGAGTCTA-3'
Shank1 RT reverse: 5'-CCTGAATCTGAGTCGTGGTAGTT-3'
Shank2 RT forward: 5'-AGAGGCCAGCTTATTCCAA-3'
Shank2 RT reverse: 5'-CAGGGGTATAGCTTCCAAGGC-3'
Gapdh RT forward: 5'-AAATGGTGAAGGTCGGTGTG-3'
Gapdh RT reverse: 5'-GCATTGCTGACAATCTTGAG-3'

References:

- Deacon, R. M., and Rawlins, J. N. (2006). T-maze alternation in the rodent. *Nat Protoc* 1, 7-12.
- Gould, T. J., Rukstalis, M., and Lewis, M. C. (2005). Atomoxetine and nicotine enhance prepulse inhibition of acoustic startle in C57BL/6 mice. *Neurosci Lett* 377, 85-90.
- Joober, R., Zarate, J. M., Rouleau, G. A., Skamene, E., and Boksa, P. (2002). Provisional mapping of quantitative trait loci modulating the acoustic startle response and prepulse inhibition of acoustic startle. *Neuropsychopharmacology* 27, 765-781.
- Logan, S. M., Partridge, J. G., Matta, J. A., Buonanno, A., and Vicini, S. (2007). Long-lasting NMDA receptor-mediated EPSCs in mouse striatal medium spiny neurons. *J Neurophysiol* 98, 2693-2704.
- Penagarikano, O., Abrahams, B. S., Herman, E. I., Winden, K. D., Gdalyahu, A., Dong, H., Sonnenblick, L. I., Gruver, R., Almajano, J., Bragin, A., et al. (2011). Absence of CNTNAP2 leads to epilepsy, neuronal migration abnormalities, and core autism-related deficits. *Cell* 147, 235-246.
- Sanjana, N. E., Cong, L., Zhou, Y., Cunniff, M. M., Feng, G., and Zhang, F. (2012). A transcription activator-like effector toolbox for genome engineering. *Nat Protoc* 7, 171-192.
- Schmeisser, M. J., Ey, E., Wegener, S., Bockmann, J., Stempel, A. V., Kuebler, A., Janssen, A. L., Udvardi, P. T., Shiban, E., Spilker, C., et al. (2012). Autistic-like behaviours and hyperactivity in mice lacking ProSAP1/Shank2. *Nature* 486, 256-260.
- Segal, M., Greenberger, V., and Korkotian, E. (2003). Formation of dendritic spines in cultured striatal neurons depends on excitatory afferent activity. *Eur J Neurosci* 17, 2573-2585.
- Tian, X., Kai, L., Hockberger, P. E., Wokosin, D. L., and Surmeier, D. J. (2010). MEF-2 regulates activity-dependent spine loss in striatopallidal medium spiny neurons. *Mol Cell Neurosci* 44, 94-108.
- Tsien, J. Z., Huerta, P. T., and Tonegawa, S. (1996). The essential role of hippocampal CA1 NMDA receptor-dependent synaptic plasticity in spatial memory. *Cell* 87, 1327-1338.
- Yin, H. H., Davis, M. I., Ronesi, J. A., and Lovinger, D. M. (2006). The role of protein synthesis in striatal long-term depression. *J Neurosci* 26, 11811-11820.